LIMNOLOGY
and
OCEANOGRAPHY: METHODS

ASLO

Limnol. Oceanogr.: Methods 13, 2015, 138–155

doi: 10.1002/lom3.10014

Toward autonomous measurements of photosynthetic electron transport rates: An evaluation of active fluorescence-based measurements of photochemistry

Greg M. Silsbe,[†*1] Kevin Oxborough,[2] David J. Suggett,[3,4] Rodney M. Forster,[5,11] Sven Ihnken,[1] Ondřej Komárek,[6] Evelyn Lawrenz,[3,6] Ondřej Prášil,[6] Rüdiger Röttgers,[7] Michal Šicner,[8] Stefan G.H. Simis,[9,12] Mark A. Van Dijk,[10] Jacco C. Kromkamp[1]

[1]Royal Netherlands Institute for Sea Research (NIOZ-YE), Yerseke, Netherlands
[2]CTG Ltd., West Molesey, United Kingdom
[3]School of Biological Sciences, University of Essex, Colchester, United Kingdom
[4]Climate Change Research Cluster, University of Technology, Sydney, New South Wales, Australia
[5]Centre for Environment, Fisheries and Aquaculture Science, Lowestoft, United Kingdom
[6]Centre Algatech, Institute of Microbiology, Academy of Sciences of the Czech Republic, Třeboň, Czech Republic
[7]Institute for Coastal Research, Helmholtz-Zentrum Geesthacht, Geesthacht, Germany
[8]Photon Systems Instruments (PSI), Drasov, Czech Republic
[9]Finish Environment Institute (SYKE), Marine Research Centre, Helsinki, Finland
[10]Royal Netherlands Institute for Sea Research (NIOZ-TX), Den Burg, Netherlands
[11]Institute of Estuarine and Coastal Studies (IECS), University of Hull, Hull, United Kingdom
[12]Plymouth Marine Laboratory, Prospect Place, The Hoe, Plymouth, United Kingdom

Abstract

This study presents a methods evaluation and intercalibration of active fluorescence-based measurements of the quantum yield (ϕ'_{PSII}) and absorption coefficient (a_{PSII}) of photosystem II (PSII) photochemistry. Measurements of ϕ'_{PSII}, a_{PSII}, and irradiance (E) can be scaled to derive photosynthetic electron transport rates (P_e), the process that fuels phytoplankton carbon fixation and growth. Bio-optical estimates of ϕ'_{PSII} and a_{PSII} were evaluated using 10 phytoplankton cultures across different pigment groups with varying bio-optical absorption characteristics on six different fast-repetition rate fluorometers that span two different manufacturers and four different models. Culture measurements of ϕ'_{PSII} and the effective absorption cross section of PSII photochemistry (σ_{PSII}, a constituent of a_{PSII}) showed a high degree of correspondence across instruments, although some instrument-specific biases are identified. A range of approaches have been used in the literature to estimate $a_{PSII}(\lambda)$ and are evaluated here. With the exception of ex situ $a_{PSII}(\lambda)$ estimates from paired σ_{PSII} and PSII reaction center concentration ([RCII]) measurements, the accuracy and precision of in situ $a_{PSII}(\lambda)$ methodologies are largely determined by the variance of method-specific coefficients. The accuracy and precision of these coefficients are evaluated, compared to literature data, and discussed within a framework of autonomous P_e measurements. This study supports the application of an instrument-specific calibration coefficient (K_R) that scales minimum fluorescence in the dark (F_0) to a_{PSII} as both the most accurate in situ measurement of a_{PSII}, and the methodology best suited for highly resolved autonomous P_e measurements.

Improved monitoring of phytoplankton productivity (PP) is a core goal across the aquatic sciences and underpins long term management plans for coastal seas and the global ocean (European Marine Board 2013). Following the success of global ocean observatory systems such as the free-drifting Argo profilers (http://www.argo.ucsd.edu/), scientists are now looking to integrate instruments that are capable of autonomous biological rate and flux measurements into environmental sensor networks (Claustre et al. 2010). Unlike traditional in vitro photosynthetic assays, active fluorescence-based photosynthetic measurements are well suited for environmental sensor networks as many of these optical instruments can operate autonomously providing high resolution in situ photosynthesis measurements.

*Correspondence: gsilsbe@gmail.com
[†]Present address: Department of Botany and Plant Pathology. Oregon State University, Corvallis, Oregon

Bio-optical models scale active fluorescence measurements to generate estimates of electron transport rates by photosystem II (P_e), whose reductant yield fuels carbon fixation and growth. The derivation of P_e is shown in Eq. 1 as the product of photon irradiance ($E(\lambda)$), the absorption coefficient of photosystem II (PSII) light-harvesting pigments ($a_{\mathrm{LHII}}(\lambda)$), and E-dependent measurements of the quantum yield of PSII photochemistry ($\phi'_{\mathrm{PSII}}(E)$), where λ represents a wavelength within the photosynthetic active radiation (PAR) spectrum (400–700 nm). As $a_{\mathrm{LHII}}(\lambda)$ is equivalent to the absorption coefficient of PSII photochemistry ($a_{\mathrm{PSII}}(\lambda)$) normalized to quantum yield of PSII photochemistry in the dark (ϕ_{PSII}), P_e is alternatively expressed following Eq. 2 (Oxborough et al. 2012, but see Suggett et al. 2010 for alternate derivations). Bio-optical measures of P_e and its constituent parameters have improved our understanding of how the environment regulates PP in the oceans (Behrenfeld et al. 2006; Moore et al. 2008b). A central consideration of fluorescence-based PP measurements is that the "photosynthetic currency" (sensu Suggett et al. 2009) of many biogeochemical models is not electrons but fixed CO_2. This requires scaling P_e measurements to the electron requirement of carbon fixation ($\Phi_{e,\mathrm{C}}$), which itself can be highly variable within and between coastal seas and oceans (Lawrenz et al. 2013). The product of P_e and $\Phi_{e,\mathrm{C}}$ integrated through space and time yields PP.

$$P_e = E(\lambda) \cdot a_{\mathrm{LHII}}(\lambda) \cdot \phi'_{\mathrm{PSII}}(E) \quad (1)$$

$$P_e = E(\lambda) \cdot a_{\mathrm{PSII}}(\lambda) \cdot \phi'_{\mathrm{PSII}}(E)/\phi_{\mathrm{PSII}} \quad (2)$$

A range of approaches have been used in the literature to estimate $a_{\mathrm{PSII}}(\lambda)$. There is no current consensus on the accuracy or intercomparability of $a_{\mathrm{PSII}}(\lambda)$ estimates across methods as their implementation is fraught with procedural inconsistencies and inherent assumptions (Suggett et al. 2004; Oxborough et al. 2012). Therefore, this study critically evaluates bio-optical models that parameterize P_e, with a key emphasis on $a_{\mathrm{PSII}}(\lambda)$ methodology. As estimates of $a_{\mathrm{PSII}}(\lambda)$ likely cause the largest uncertainty in P_e measurements (Silsbe et al. 2012), it is not clear if and how the growing number of P_e datasets, and by extension $\Phi_{e,\mathrm{C}}$ datasets, can be reconciled. This study builds on a previous methods evaluation (Suggett et al. 2004) by incorporating recent advances in bio-optical instrumentation and algorithms (Röttgers and Doerffer 2007; Oxborough et al. 2012). Synchronous fast-repetition rate fluorescence (FRRf) measurements were made on six different instruments that span two different manufacturers and four different models. Thus, this study also constitutes novel and systematic intercalibration measurements. Bio-optical estimates of $a_{\mathrm{PSII}}(\lambda)$ and $\phi'_{\mathrm{PSII}}(E)$ were evaluated using 10 phytoplankton cultures across different pigment groups with varying bio-optical absorption characteristics (Johnsen and Sakshaug 2007).

Table 1 provides a conceptual overview of the four most commonly used methods that, in conjunction with active fluorescence measurements, seek to measure $a_{\mathrm{PSII}}(\lambda)$. All symbols and definitions are presented in Table 2. For clarity, method-specific subscripts are appended to $a_{\mathrm{PSII}}(\lambda)$ in Table 1 and throughout this manuscript. For each method, Table 1 lists its inherent assumptions, any ancillary (nonactive fluorescence) measurement dependencies, states each method's spectral domain and spatiotemporal resolution. In Table 1, λ_{ex} represents the excitation spectrum of a given active fluorometer. Our study used both older FRR fluorometer models with a single set of excitation light emitting diodes (LEDs) constrained within the blue spectrum and newer models with multiple excitation wavebands that provide more spectrally explicit $a_{\mathrm{PSII}}(\lambda_{\mathrm{ex}})$ measurements (see Materials and Procedure). Therefore, for simplicity the intercalibration measurements presented below are limited to fluorescence measured within the blue spectrum.

Direct measures of $a_{\mathrm{PSII}}(\lambda)$ can only be derived from the product of the functional PSII reaction center concentration ([RCII]) and the effective absorption cross section of PSII ($\sigma_{\mathrm{PSII}}(\lambda_{\mathrm{ex}})$), as measured by oxygen flash yields and single-turnover active fluorescence, respectively (Suggett et al. 2004). Oxygen flash yield measurements are time consuming and require highly concentrated algal samples (>1 g chlorophyll a m^{-3}). Consequently direct $a_{\mathrm{PSII}}(\lambda_{\mathrm{ex}})$ measures have been rarely made for natural phytoplankton samples (Moore et al. 2006; Suggett et al. 2006; Oxborough et al. 2012) and are not a viable option for routine in situ measurements. This study, therefore, uses direct $a_{\mathrm{PSII}}(\lambda_{\mathrm{ex}})$ measures as a benchmark against which to evaluate other $a_{\mathrm{PSII}}(\lambda_{\mathrm{ex}})$ methods shown in Table 1.

Table 1. Overview of four bio-optical methods that quantify $a_{\mathrm{PSII}}(\lambda)$ in conjunction with FRR fluorometry. All terms and definitions are defined in Table 2

Method Symbol	Derivation	Assumed Constants	Ancillary Measurements	Spectral Domain	Spatiotemporal Resolution
Direct Measures $a_{\mathrm{PSII}}(\lambda)$	$[\mathrm{RCII}] \cdot \sigma_{\mathrm{PSII}}(\lambda_{\mathrm{ex}})$	None	[RCII]	Confined to λ_{ex}	Dictated by [RCII]
Fixed n_{PSII} $a_{\mathrm{PSII.npsii}}(\lambda)$	$n_{\mathrm{PSII}} \cdot [\mathrm{chl}\,a] \cdot \sigma_{\mathrm{PSII}}(\lambda_{\mathrm{ex}})$	n_{PSII}	[chl a]	Confined to λ_{ex}	Dictated by [chl a]
Optical $a_{\mathrm{PSII.opt}}(\lambda)$	$a_\phi(\lambda) \cdot \mathrm{fAQ}_{\mathrm{PSII}} \cdot \phi_{\mathrm{PSII}}$	$\mathrm{fAQ}_{\mathrm{PSII}}$	$a_\phi(\lambda)\{F_{\mathrm{PSII}}(\lambda), [c_i]\}$	Dictated by $a_\phi(\lambda)$	Dictated by $a_\phi(\lambda)$
Fixed K_R $a_{\mathrm{PSII.Kr}}(\lambda)$	$F_0(\lambda_{\mathrm{ex}}) \cdot K_R$	K_R.	None	Confined to λ_{ex}	Dictated by FRRF

Table 2. List of symbols

Symbol	Definition	Units
$a_i^*(\lambda)$	Mass-specific absorption coefficient of pigment *i*	m^2 mg pigment^{-1}
$a_{LHII}(\lambda)$	Absorption coefficient of photosystem II (PSII) light harvesting pigments	m^{-1}
$\hat{a}_{LHII}$	Mean $a_{LHII}(\lambda)$ over the PAR spectrum	m^{-1}
$a_{NP}(\lambda)$	Absorption coefficient nonphotosynthetic pigments	m^{-1}
$a_{LH}(\lambda)$	Absorption coefficient of PSII and PSI light harvesting pigments	m^{-1}
$a_{PSII}(\lambda)$	Absorption coefficient PSII photochemistry	m^{-1}
$a_{sol}(\lambda)$	Unpackaged pigment absorption coefficient	m^{-1}
$a_{std}^*(\lambda)$	Mass-specific absorption coefficient of a pigment standard	m^2 mg^{-1}
$\hat{a}_{std}^*$	Mean $a_{std}^*(\lambda)$ over the PAR spectrum	m^{-1}
$a_\phi(\lambda)$	Absorption coefficient of phytoplankton pigments	m^{-1}
$[c_i]$	Concentration of pigment *i*	mg pigment m^{-3}
[chl *a*], [chl a_{std}]	Concentration of chl *a* in vivo and in 90% acetone	mg chl *a* m^{-3}
$E(\lambda_{ac})$	Actinic irradiance during a fluorescence light curve	μmol photons m^{-2} s^{-1}
E_K	Light saturation parameter of a fluorescence light curve	μmol photons m^{-2} s^{-1}
$E_{LED}(\lambda_{ex})$	Instrument-specific excitation energy at wavelength λ_{ex}	mol photons m^{-2} s^{-1}
fAQ_{PSII}	Fraction of absorbed photons directed toward PSII	Dimensionless
$F_{DOM}(\lambda_{ex})$	Fluorescence of sample filtrate	Dimensionless
$F_{PSII}(\lambda)$	PSII in vivo fluorescence	mol photons m^{-2} s^{-1}
$F_0(\lambda_{ex})$, $F_0'(\lambda_{ex})$	Minimum flux of fluorescence when all reaction centers are in the dark and light regulated state	Dimensionless
$F_M(\lambda_{ex})$, $F_M'(\lambda_{ex})$	Maximum flux of fluorescence when all reaction centers are in the dark and light regulated state	Dimensionless
$F_0^{std}(\lambda_{ex})$	Minimum fluorescence normalized to $E_{LED}(\lambda_{ex})$ and instrument gain	Dimensionless
K_R	Instrument-specific coefficient that scales $F_0^{std}(\lambda_{ex})$ to $a_{PSII}(\lambda_{ex})$	m^{-1}
K_{std}	As above, but derived from [chl a_{std}] and instrument optics	m^{-1}
n_{PSII}	RCII per chl *a*	RCII (chl *a*)$^{-1}$
p	Connectivity parameter	Dimensionless
P_e	Photosynthetic electron transport rate	μmol e^- m^{-3} s^{-1}
Q_{abs}^*	Pigment packaging index	Dimensionless
[RCII]	Concentration of PSII reaction centres	mol RCII m^{-3}
SCF	Spectral correction factor to scale $a_{PSII}(\lambda_{ex})$, $\sigma_{PSII}(\lambda_{ex})$ over a PAR spectrum	Dimensionless
SCF_{std}	Spectral correction factor to scale $F_0^{std}(\lambda_{ex})$ over a PAR spectrum	Dimensionless
T_{em}	Transmission spectrum of FRRf emission window	Dimensionless
λ_{ex}, λ_{em}	Instrument-specific excitation spectrum, emission spectrum	Nm
ϕ_f	Quantum yield of fluorescence	Dimensionless
ϕ_f^{PSII}	Quantum yield of chlorophyll fluorescence for open PSII reaction centres	Dimensionless
ϕ_f^{std}	Quantum yield of chlorophyll fluorescence in 90% acetone	Dimensionless
ϕ_P	Quantum yield of charge separation	Dimensionless
ϕ_{PSII}, ϕ_{PSII}'	Quantum yield of PSII photochemistry in the dark, under actinic irradiance	Dimensionless
$\Phi_{e,C}$	Electron requirement for carbon fixation	mol C (mol e)$^{-1}$
$\Phi_F(\lambda_{em})$	FRRf-specific function representing the spectral dependence of emission detection	Dimensionless
$\sigma_{PSII}(\lambda_{ex})$	Effective absorption cross section of PSII photochemistry	nm^2

i refers to the photosynthetic pigments chl *a*, chl *b*, chl *c*, fucoxanthin, and peridin, and non-photosynthetic pigments neoxanthin, violaxanthin, diadinoxanthin, diatoxanthin, lutein, zeaxanthin, and β-carotene. *denotes normalization to pigment *i*.

The most widely used parameterization of $a_{PSII}(\lambda)$ to date (see Lawrenz et al. 2013) is the "fixed n_{PSII}" method shown in Table 1 and herein denoted $a_{PSII.npsii}(\lambda)$. In this approach, $a_{PSII.npsii}(\lambda)$ is calculated as the product of a chlorophyll *a* concentration ([chl *a*]) as measured by pigment extraction, an assumed molar ratio of functional PSII reaction centers to chl *a* (n_{PSII}), and the absorption cross section of PSII photochemistry ($\sigma_{PSII}(\lambda_{ex})$) derived from single-turnover active fluorescence. The accuracy of this approach is dependent on the assumption that n_{PSII} does not deviate from its assumed value (nominally 2.0×10^{-3} mol RCII (mol chl *a*)$^{-1}$ following Kolber and Falkowski (1993)). While the potential inaccuracy of the "fixed n_{PSII}" method has long been recognized (Suggett et al. 2004), a

Table 3. List of phytoplankton cultures employed in this study

Species	Symbol	Strain	Media
Chaetocorus muelleri	*Cm*	Algalink	Filtered sea water
Ditylum brightwellii	*Db*	CCY1202	F/2+Si
Emiliania huxyleyi	*Eh*	CCY0388	MDV
Phaeocystis globosa	*Pg*	CCY0803	L1+
Prorocentrum minimum	*Pm*	CCY1203	K minimum
Skeletonema costatum	*Sc*	CCY9929	JL1++
Tetraselmis striata	*Ts*	CCY9927	MDV
Thalassiosira pseudonana	*Tp*	CCY9928	MDV
Thalassiosira pseudonana	*Tp-Fe*	CCY9928	MDV (Fe deplete)
Thalassiosira weissflogii	*Tw-Fe*	CCY1204	F/2+Si (Fe deplete)

less noted drawback is this method's need for independent [chl *a*] measurements. As [chl *a*] is typically measured from discrete water samples, it is the frequency of [chl *a*] measures that ultimately dictates the spatiotemporal resolution of the "fixed n_{PSII}" method.

The second most common approach to estimate $a_{PSII}(\lambda)$ is referred to as an "optical" method in Table 1 and is herein denoted $a_{PSII.opt}(\lambda)$. This method often supplements pulse amplitude modulated fluorescence measurements that cannot resolve $\sigma_{PSII}(\lambda_{ex})$ (Hartig et al. 1998; Gilbert et al. 2000; Kromkamp et al. 2008). This method uses the optical phytoplankton pigment absorption coefficient ($a_\phi(\lambda)$) that represents the sum of absorption of light-harvesting pigments associated with both PSII ($a_{LHII}(\lambda)$) and photosystem I ($a_{LHI}(\lambda)$) as well as nonphotosynthetic pigments ($a_{NP}(\lambda)$). The key uncertainty with this method originates from estimating the fraction of absorbed quanta directed toward PSII (fAQ_{PSII}), a parameter that quantifies the ratio of $a_{LHII}(\lambda)$ to $a_\phi(\lambda)$ (Johnsen and Sakshaug 2007). Some studies assume fAQ_{PSII} is 0.50, such that $a_{LHII}(\lambda)=a_\phi(\lambda)\times 0.5$ (Gilbert et al. 2000; Kromkamp et al. 2008). Other studies seek to constrain fAQ_{PSII} by measuring pigment concentrations ($[c_i]$, where i represents a specific pigment) to first remove $a_{NP}(\lambda)$ from $a_\phi(\lambda)$ as well as incorporating spectral fluorescence measurements ($F_{PSII}(\lambda)$) as a proxy for the spectral shape of $a_{LHII}(\lambda)$ (Suggett et al. 2004; Johnsen and Sakshaug 2007). As $a_{LHII}(\lambda)$ measurements represent optical absorption, estimates are multiplied by ϕ_{PSII} to arrive at functional PSII absorption ($a_{PSII.opt}(\lambda)$). While fAQ_{PSII} is likely the largest source of uncertainty in optical derivations of $a_{PSII.opt}(\lambda)$, measurement of $a_\phi(\lambda)$ alone can also represent a source of error (Röttgers and Gehnke 2012). The vast majority of studies that have adopted this optical approach determine $a_\phi(\lambda)$ using the quantitative filter technique (QFT, Mitchell 1990). Thus, while $a_{PSII.opt}(\lambda)$ measurements are spectrally resolved, the spatial resolution of this method is dictated by the frequency of water samples. That said, the recent introduction of flow-through point-source integrating-cavity absorption meters (PSICAM) permit spatially resolved $a_\phi(\lambda)$ estimates as these instruments can be incorporated into ferry boxes and other mobile sampling platforms (Röttgers et al. 2007; Moore et al. 2008a). However, the only study reporting unattended PSICAM measurements notes that persistent contamination of the instrument's wall causes sensor drift (Wollschläger et al. 2013).

Finally, the recently proposed "absorption method" (Oxborough et al. 2012), which is described here as the "K_R" method, derives $a_{PSII}(\lambda_{ex})$ from FRRf measurements alone (Oxborough et al. 2012) and is herein denoted $a_{PSII.Kr}(\lambda)$. This method scales the minimal fluorescence yield measured in the dark ($F_0(\lambda_{ex})$) to $a_{PSII.Kr}(\lambda)$ through an instrument-specific proportionality constant (K_R) whose variance appears limited (Oxborough et al. 2012). As outlined below in Materials and Procedures, K_R invariance assumes that the quantum yield of PSII fluorescence (ϕ_f) and PSII photochemistry (ϕ_{PSII}) in the dark are proportional. As $F_0(\lambda_{ex})$ measurements are also dependent on instrument settings (photomultiplier gain, photon output of excitation light), this method also has an operational assumption that $F_0(\lambda_{ex})$ can be accurately normalized to these settings. Testing these instrument-dependent assumptions is an important aim of this study. Most FRRf models can operate autonomously with unparalleled resolution. This method, therefore, promises to be the most suitable for unattended spatially and temporally resolved photosynthesis measurements.

Materials and procedures

Phytoplankton cultures

Nine monospecific cultures and one culture from a commercial bioreactor (Algaelink NV, Yerseke NL) were used in this study (Table 3). All cultures were grown in batch mode with a 14 : 10 hour light : dark cycles ($80\,\mu mol\,m^{-2}\,s^{-1}$ PAR) at 18°C. Four weeks prior to measurements, two milliliters of each stock culture was transferred into 100 mL of fresh media, with another transfer of 10 mL into 100 mL of fresh media five days prior to measurements. Two of the cultures were grown in media without any iron and are denoted *Tp-Fe* and *Tw-Fe*.

Fast-repetition rate fluorescence (FRRf)

The six different FRRFs used in this study included three different Chelsea Technologies Group models (CTG, Surrey, UK), the MKI, MKII, and MKIII (FastOcean), and a Photon Systems Instruments (PSI, Drasov, CZ) OnlineFlow Fluorometer FFL-2012. These instruments broadly reflect the diversity of FRRfs used by the scientific community. For example, 12 of the 14 studies cited in the meta-analysis of Lawrenz et al. (2013) used a Chelsea MKI or MKII FRRf; the other two studies used a FIRe benchtop instrument (Satlantic, Halifax, Canada) and $FRR^{Diving\ Flash}$ (Kimoto Electric Co., Osaka, Japan). The MKIII and PSI FRRf are newer instruments and, therefore, were not cited in Lawrenz et al.'s (2013) meta-analysis. Table 4 lists the peak excitation wavelength(s),

Table 4. Single-turnover FRRfs used in the study. All instruments are herein referred to by their stated abbreviation. S.N. is the instrument's serial number. $E_{LED}(\lambda_{ex})$ denotes the peak wavelength(s) of each instruments excitation waveband(s). For each instrument, the emission filters and photomultiplier tube (PMT) are stated. RG665 are Schott filters, 682AF30 filters are supplied from Horiba Scientific (Edison NJ, USA), BPF10-680 filters are from Corion Corporation (Holliston, Massachusetts), and FB680-10 filters are from Thorlabs (Newton, New Jersey). All PMTs are manufactured by Hamamatsu (Hamamastu, Japan)

Instrument	Abbreviation	S.N.	$E_{LED}(\lambda_{ex})$ (nm)	Emission Filters	PMT
FastOcean	MKIII		443, 515, 635	RG665, 682AF30	R9880U-20
MKII FASTtracka	$MKII_a$	09-7018	470	RG665, 682AF30	R7800U-02
MKII FASTtracka	$MKII_b$	08-6667	470	RG665, 682AF30	R7800U-02
MKI FASTtracka	MKI_a	182059	462	RG665, BPF10-680	R928
MKI FASTtracka	MKI_b	182011	462	RG665, BPF10-680	R928
OnlineFlow	PSI	OFF-001	455, 630	FB680-10	S5106

emission filters, and photomuliplier tube (or photodiode for the PSI FRRf) for the instruments used in the study. Only 5 of the 10 cultures were measured on the FRRf denoted $MKII_a$, however, they compromised phytoplankton species of different pigment types ensuring an adequate range for comparative measures (see Assessment). Prior to all FRRf measurements, cultures were diluted in their respective medium, so resultant [chl *a*] fell within fluorometers' calibration range (3–30 mg chl *a* m^{-3}). That said, inspection of the raw fluorescence data for the MKI_b suggested 4 of the 10 cultures (*Tp-Fe, Tw-Fe, Tp*, and *Ts*) exceeded the dynamic range of this particular instrument. Therefore, data for these four cultures for the MKI_b are omitted in the Assessment.

Fluorescence light curves (FLCs) were measured on all instruments with the standard single-turnover induction protocol (Suggett et al. 2004; Oxborough et al. 2012). Induction curves were fit to the four parameter model of Kolber et al. (1998) to yield the minimum and maximum fluorescence ($F_0(\lambda_{ex})$ and $F_M(\lambda_{ex})$), the absorption cross section of PSII ($\sigma_{PSII}(\lambda_{ex})$), and the connectivity parameter (p). For the MKIII and MKII fluorometers, induction curves were fit with the manufacturer's FastPro software. For the PSI FRRf, single-turnover induction curves were fit to the four parameter Kolber et al. (1998) model using a script written in the open source statistical program R (R Development Core Team 2011) provided by PSI. For the MKI fluorometers, induction curves were fit to the Kolber et al. (1998) model using a Matlab script (V6) described in Laney and Letelier (2008). Visual inspection of induction curves revealed that the MKI fluorometers were generally noisier than other instruments. For quality control, any MKI induction curves where $\chi^2 > 0.05$ (as quantified by the Matlab V6 script) were rejected. To ensure that different induction curve algorithms did not induce any bias in FRRf data, a subset of induction curves ($n = 50$) fitted with FastPro 8 were exported and fitted with the R and Matlab V6 script. A comparison of the fluorescence parameters between fitting software showed no significant difference in model parameters ($p < 0.01$, data not shown).

Fluorescence normalization

Fluorescence measures are not only dependent on the properties of a given sample but also vary with the instrument's photomultiplier gain and excitation energy ($E_{LED}(\lambda_{ex})$) settings. During factory calibration, FRRfs measurements are routinely performed on chl *a* standards in 90% acetone ([chl a_{std}]) across gain and $E_{LED}(\lambda_{ex})$ settings. These measurements lead to a set of coefficients that permit $F_0(\lambda_{ex})$ and $F_M(\lambda_{ex})$ to be normalized to both gain and $E_{LED}(\lambda)$. All five Chelsea instruments used in this study had been factory calibrated within a year of this study, and the PSI fluorometer underwent a similar [chl a_{std}] calibration after the measurements of this study. All $F_0(\lambda_{ex})$ and $F_M(\lambda_{ex})$ measurements in this study have been normalized to [chl a_{std}] following instrument-dependent calculations outlined in Supporting Information. Normalized measurements are herein denoted $F_0^{std}(\lambda_{ex})$ and $F_M^{std}(\lambda_{ex})$. Critically, $F_0^{std}(\lambda_{ex})$ and $F_M^{std}(\lambda_{ex})$ have been normalized such that resultant values are equivalent to [chl a_{std}]. In other words, and if the calibration is done correctly, an FRRf calibrated with a chl *a* standard in 90% acetone whose concentration is 10 μg chl *a* L^{-1}, will return $F_0^{std}(\lambda_{ex})$ and $F_M^{std}(\lambda_{ex})$ values of 10 μg chl *a* L^{-1} across all gain and $E_{LED}(\lambda_{ex})$ settings (note that because the standard should not show any fluorescence induction $F_0^{std}(\lambda_{ex})$ and $F_M^{std}(\lambda_{ex})$ are equivalent). This fluorescence normalization is critical to validating the absorption (fixed K_R) method discussed in greater detail below.

Background fluorescence

After each FLC, sample filtrate (Whatman GF/F under low vacuum pressure) of the corresponding culture was measured on each FRRf. This data was visually inspected to ensure no fluorescence induction, such that $F_0^{std}(\lambda_{ex})$ and $F_M^{std}(\lambda_{ex})$ are equivalent indicating the absence of phytoplankton in the filtrate. The mean $F_0^{std}(\lambda_{ex})$ and $F_M^{std}(\lambda_{ex})$ of this filtrate was averaged into a single value ($F_{CDOM}(\lambda_{ex})$) for each instrument and culture. Across all instruments and cultures, $F_{CDOM}(\lambda_{ex})$ has been subtracted from all $F_0^{std}(\lambda_{ex})^{(')}$ and $F_M^{std}(\lambda_{ex})^{(')}$ sample measurements. When expressed as a percentage of $F_0^{std}(\lambda_{ex})$,

$F_{CDOM}(\lambda_{ex})$ was less than 6% for all nine monospecific cultures (average 3%) but was between 10% and 13% for the bioreactor sample (*Chaeotecorus muelleri*).

Fluorescence light curves (FLCs)

For all Chelsea FRRfs, each FLC consisted of five minutes of dark measurements followed by a series of five minute steps over which actinic photon irradiance ($E(\lambda_{ac})$) was incrementally increased (range 5–600 μmol m^{-2} s^{-1}). For the PSI FRRf, the duration of each FLC step varied from 150 s to 250 s depending on the culture, over which $E(\lambda_{ac})$ was incrementally increased (range 5–500 μmol m^{-2} s^{-1}). For the MKIII and MKII FRRfs, FLCs were acquired using the FastAct laboratory system (CTG, Surrey, UK). For the MKI FRRfs, diluted cultures were dispensed into culture vessels, placed adjacent to the emission and excitation windows, and exposed to a programmable LED panel (PSI SL 3500, Drasov, CZ). For the PSI fluorometer, FLCs were measured with the instrument's built-in actinic irradiance source. The light dependency of the quantum yield of PSII ($\phi'_{PSII}(E)$) was modeled for each instrument and culture by fitting $\phi'_{PSII}(E)$ to an *E*-normalized PE model (Webb et al. 1974) following Silsbe and Kromkamp (2012) to derive the light saturation parameter (E_K). Actinic irradiance spectra ($E(\lambda_{ac})$) differed between instruments with the FastAct system (MKIII and MKII) producing a cool white spectrum, the MKI having a warm white spectrum, and PSI using a blue spectrum ($\lambda_{max} = 455$ nm). To compare E_K between instruments, spectral correction factors were applied as described below.

Pigment concentrations

Pigment concentrations on diluted cultures used for the FRRf measurements were collected on Whatman GF/F filters and held at –80°C until analysis. Filters were extracted in 90% acetone and analyzed using reverse phase high-performance liquid chromatography (HPLC) as described by Rijstenbil (2003) and references therein. Chl *a* concentrations on concentrated samples used for the [RCII] measurements (see below) were collected on Whatman GF/F filters and immediately extracted in a mixture of 90% acetone and 10% dimethylsulfoxide (Shoaf and Lium 1976). Extracts were measured on a scanning spectrophotometer (Varian Cary BIO-100, Palo Alto) and [chl *a*] was calculated from absorbance following Ritchie (2006).

Reaction centre II concentrations

[RCII] was determined using the oxygen flash yield technique on concentrated cultures (Mauzerall and Greenbaum 1989) in parallel with FRRf measurements. Cultures were concentrated through low-pressure filtration (~ 2 mm Hg) over 47 mm polycarbonate membrane filters (0.2 μm), then gently resuspended in five milliliters of filtrate. Aliquots of two milliliters were then transferred into an air-tight reaction chamber, and the remaining sample volume reserved for pigment and cell count analysis. The reaction chamber was surrounded by a transparent water jacket connected to a circulating water bath set to 18°C. Oxygen (O_2) concentrations within the chamber were measured with a Clarke-type electrode housed within a DW1 liquid-phase oxygen electrode chamber (Hansatech Instruments, King's Lynn, UK) calibrated against 100% and 0% oxygen concentrations. A single-turnover saturation flash system consisted of 200 blue LEDs surrounding a reaction chamber was controlled by a NI-DAQ (National Instruments, Texas) high-speed timer card. The flash system generated 10-minute sequences of 20, 30, 40, and 50 flashes s^{-1} interspersed with 10-minute dark sequences. A mean O_2 evolution rate per flash (P_{O_2}) was calculated for each flash sequence, and a single O_2 respiration rate (R_{O_2}) was averaged from all dark measurements (R_{O_2} coefficient of variance between sequences < 8%). For each of the four 10-minute sequences, [RCII] is calculated as $(P_{O_2} - R_{O_2}) \times 4$ mol RCII (mol O_2)$^{-1}$. The mean and standard error of the four [RCII] estimates are reported for each culture. Further details can be found in Suggett et al. (2004, 2007). All [RCII] measurements presented below are divided by a dilution factor calculated as the ratio of [chl *a*] measurements on concentrated and diluted samples.

Spectral absorption

The phytoplankton pigment absorption coefficient ($a_\phi(\lambda)$) was determined on two instruments: (1) The QFT as outlined in Röttgers and Gehnke (2012) and (2) A PSICAM (TRIOS, Rastede, Germany) as described in Röttgers et al. (2007) and Röttgers and Doerffer (2007). QFT measurements were prepared by filtering 50–300 mL of the culture onto 47-mm GF/F (Whatman) filters, then placing the filters on a center-mount holder inside a large integrating sphere (Labsphere DRA-CA-3300, North Sutton) of a Cary BIO-100 dual-beam spectrophotometer (Varian, Palo Alto). The optical density (OD) of the filters were measured against reference filters wetted with a few drops of culture medium in the wavelength region of 300–800 nm (slit width: 2 nm) to obtain $a_P(\lambda)$. After each measurement the filter was wetted with a 10% NaOCl solution (Tassan and Ferrari 1995), quickly dried on a tissue, and the remaining NaOCl was oxidized with a few drops of a 10% H_2O_2 solution. The OD of the bleached filter was measured as described above to determine nonalgal matter absorbance ($A_{NAP}(\lambda)$). PSICAM measurements of the culture suspension in the wavelength range of 400–700 nm resulted in the sum of absorption by particulate and dissolved matter. Therefore, additional measurements of culture filtrate (0.2 μm) were subtracted from the suspension measurements to obtain $a_p(\lambda)$. $a_\phi(\lambda)$ is calculated as $a_\phi(\lambda) = 2.303 \times (A_P(\lambda) - A_{NAP}(\lambda)) \times l^{-1} \times \beta^{-1}$, where 2.303 is the conversion from a base-10 to a natural logarithm, l is the path length calculated from the filtration volume as $l = V/A$, and β is the path length amplification coefficient (4 and 4.5 for the integrated sphere/scanning spectrophotometer and PSICAM, respectively, Röttgers and Gehnke 2012). The

correlation coefficient of the linear regression for $a_\phi(\lambda)$ measures between the two instruments exceeded 0.97 across all cultures and the grand mean ± standard error of the slopes of the linear regressions is 0.98 ± 0.03. As the PSICAM can in principle be operated autonomously on moorings and profilers (Röttgers et al. 2007), all measures of $a_\phi(\lambda)$ presented below are from this instrument.

Fluorescence excitation spectra

Phytoplankton cultures were treated with 20 μM 3-(3,4-dichlorophenyl)-1,1-dimethylurea (DCMU, Sigma-Aldrich) and maintained in the light for five minutes to saturate PSII reaction centers and minimize reabsorption of fluoresced photons (e.g., Johnsen and Sakshuag 2007). Cultures were then dispensed in a 10 mm quartz cuvette and placed within in a scanning spectrofluorometer (Cary Eclipse, Agilent, Santa Clara). Fluorescence excitation spectra ($F_{\mathrm{PSII}}(\lambda)$) were measured by setting the emission spectrum to 682 nm and varying the excitation spectrum between 400 nm and 650 nm. To account for spectral differences in excitation energy, $F_{\mathrm{PSII}}(\lambda)$ was normalized to a wavelength-specific quantum correction factor following Kopf and Heinze (1984).

Methods to determine $a_{\mathrm{PSII}}(\lambda)$

Direct measures and "fixed n_{PSII}" measures of $a_{PSII}(\lambda)$

All equations related to the derivation of $a_{\mathrm{PSII}}(\lambda)$ across methodologies are presented in Table 5. Direct measures of $a_{\mathrm{PSII}}(\lambda_{\mathrm{ex}})$ were calculated as the product of [RCII], $\sigma_{\mathrm{PSII}}(\lambda_{\mathrm{ex}})$ measurements from each instrument, and a unit conversion coefficient ($6.022 \times 10^5 = 6.022 \times 10^{23}\,\mathrm{mol}^{-1} \times 10^{-18}\,\mathrm{m}^2\,\mathrm{nm}^{-2}$, Eq. 3). "Fixed n_{PSII}" measures of $a_{\mathrm{PSII.npsii}}(\lambda_{\mathrm{ex}})$ are calculated as the product of an assumed n_{PSII} value (0.002 mol RCII mol chl a^{-1}), [chl a], $\sigma_{\mathrm{PSII}}(\lambda_{\mathrm{ex}})$, and a unit conversion coefficient ($0.674 = 1.12 \times 10^{-6}$ mol chl a (mg chl a)$^{-1} \times 6.022 \times 10^{23}$ mol$^{-1} \times 10^{-18}\,\mathrm{m}^2\,\mathrm{nm}^{-2}$, Eq. 4). The departure of n_{PSII} from its assumed value is presented in the Assessment. Following Eq. 5, n_{PSII} was calculated as the product of [RCII] normalized to [chl a] and a coefficient for unit conversion (8.925×10^5 mg chl a (mol chl a)$^{-1}$).

Optical measures of $a_{PSII.opt}(\lambda)$

Various methods present in the literature derive $a_{\mathrm{PSII.opt}}(\lambda)$ from measurements of $a_\phi(\lambda)$ (Johnsen and Sakshaug 2007; Kromkamp et al. 2008). Here, we follow the method of Suggett et al. (2004) that (1) calculates the optical absorption of photosynthetic pigments ($a_{\mathrm{ps}}(\lambda)$) by subtracting $a_{\mathrm{np}}(\lambda)$ from $a_\phi(\lambda)$, (2) derives $a_{\mathrm{LHII}}(\lambda)$ by scaling $F_{\mathrm{PSII}}(\lambda)$ to $a_{\mathrm{ps}}(\lambda)$ assuming $\mathrm{fAQ}_{\mathrm{PSII}}$ across the PAR spectrum is 0.5, and (3) multiplies $a_{\mathrm{LHII}}(\lambda)$ by ϕ_{PSII} to yield $a_{\mathrm{PSII.opt}}(\lambda)$. Pigment-specific absorption coefficients, $a_i(\lambda)$, were derived as the product of the pigment's in vivo absorption spectrum ($a_i^*(\lambda)$) and concentration [c_i] (Eq. 6). Following Bricaud et al. (2004), [c_i] represents HPLC measures of chl a, chl b, chl c, photosynthetic carotenoids (psc), photoprotective carotenoids (ppc), or pheophytin a (pheo), with corresponding $a_i^*(\lambda)$ spectra taken from Bidigare et al. (1990). The unpackaged pigment absorption coefficient ($a_{\mathrm{sol}}(\lambda)$) is the sum of $a_i(\lambda)$ for the six pigments classes (Eq. 7). The dimensionless pigment packaging parameter ($Q^*_{\mathrm{abs}}(\lambda)$) was derived as the ratio of $a_\phi(\lambda)$ to $a_{\mathrm{sol}}(\lambda)$ (Eq. 8), and $a_{\mathrm{ps}}(\lambda)$ is calculated by subtracting $a_{\mathrm{np}}(\lambda) \times Q^*_{\mathrm{abs}}(\lambda)$ from PSICAM measures of $a_\phi(\lambda)$ (Eq. 9). Measurements of $F_{\mathrm{PSII}}(\lambda)$ were then scaled to $a_{\mathrm{ps}}(\lambda)$ to derive $a_{\mathrm{LHII}}(\lambda)$ in a two-step process. First, as $F_{\mathrm{PSII}}(\lambda)$ was measured between 400 nm and 650 nm, we assumed the spectral shape of $F_{\mathrm{PSII}}(\lambda_{650\rightarrow700\mathrm{nm}})$ was equivalent to $a_{\mathrm{PS}}(\lambda_{650\rightarrow700\mathrm{nm}})$. Second, $F_{\mathrm{PSII}}(\lambda)$ was normalized to $a_{\mathrm{PS}}(\lambda)$ assuming $\mathrm{fAQ}_{\mathrm{PSII}}$ across the PAR spectrum is 0.5 (Eq. 10). Finally, the product of $a_{\mathrm{LHII}}(\lambda)$ and ϕ_{PSII} yields $a_{\mathrm{PSII.opt}}(\lambda)$ (Eq. 11). To test the assumption that $\mathrm{fAQ}_{\mathrm{PSII}}$ equals 0.5, $\mathrm{fAQ}_{\mathrm{PSII}}(\lambda_{\mathrm{ex}})$ was estimated for each culture as the ratio of direct $a_{\mathrm{PSII}}(\lambda_{\mathrm{ex}})$ measurements (Eq. 3) to $a_{\mathrm{ps}}(\lambda_{\mathrm{ex}}) \times \phi_{\mathrm{PSII}}$ (Eq. 12). As estimates of $\mathrm{fAQ}_{\mathrm{PSII}}(\lambda_{\mathrm{ex}})$ are spectrally explicit, the mean value across the PAR spectrum ($\mathrm{fAQ}_{\mathrm{PSII}}$) was calculated following Eq. 13.

Fixed K_R measures of $a_{PSII}(\lambda)$

Here, we briefly summarize the theory and derivation of the factor K_R that scales $F_0(\lambda_{\mathrm{ex}})$ to $a_{\mathrm{PSII.Kr}}(\lambda_{\mathrm{ex}})$ (for a complete overview see the original article, Oxborough et al. 2012). The quantum yields of fluorescence (ϕ_{f}) and photochemistry (ϕ_{p}) can be expressed as a function of the rate constants for photochemistry (k_{p}), fluorescence (k_{f}), and nonradiative decay (k_{d}). These equations (Eqs. 14, 15) demonstrate the proportional impact that k_{d} has on ϕ_{f} and ϕ_{p}. Consequently, for a given $k_{\mathrm{f}}/k_{\mathrm{p}}$ ratio, any change in k_{d} will result in proportional changes in ϕ_{f} and ϕ_{p}. Considering an optically thin phytoplankton sample with open RCIIs in the dark-adapted state, the measured fluorescence ($F_0(\lambda_{\mathrm{ex}})$) of this sample is proportional to the product of $a_{\mathrm{LHII}}(\lambda_{\mathrm{ex}})$, $E_{\mathrm{LED}}(\lambda_{\mathrm{ex}})$, and ϕ_{f} (Eq. 16). The substitution of functional ($a_{\mathrm{PSII}}(\lambda_{\mathrm{ex}}) \cdot \phi_{\mathrm{p}}{}^{-1}$) for optical ($a_{\mathrm{LHII}}(\lambda_{\mathrm{ex}})$) absorption in Eq. 16 yields Eq. 17, which links $F_0(\lambda_{ex})$ and $a_{\mathrm{PSII}}(\lambda_{\mathrm{ex}})$ through the proportionality constant $k_{\mathrm{f}}/k_{\mathrm{p}}$. The coefficient K_R in Eq. 18 represents the inverse of $k_{\mathrm{f}}/k_{\mathrm{p}}$, scaling $F_0(\lambda_{\mathrm{ex}})$ measurements to $a_{\mathrm{PSII}}(\lambda_{\mathrm{ex}})$. In Eq. 18, the units for K_R are photons m^{-3} s^{-1} as originally derived by Oxborough et al. (2012). In this study, $F_0^{\mathrm{std}}(\lambda_{\mathrm{ex}})$ substitutes $F_0(\lambda_{\mathrm{ex}})$ to account for varying instrument settings (Eq. 19), so the units for K_R are m^{-1}. K_R values are derived as the ratio of direct $a_{\mathrm{PSII}}(\lambda_{\mathrm{ex}})$ measurements (Eq. 3) to $F_0^{\mathrm{std}}(\lambda_{\mathrm{ex}})$ (Eq. 20). For a given instrument, $a_{\mathrm{PSII.Kr}}(\lambda_{\mathrm{ex}})$ is calculated as the product of $F_0^{\mathrm{std}}(\lambda_{\mathrm{ex}})$ and the mean K_R derived from all measurements on cultures (Eq. 21).

K_R validation

This study extends the original analysis presented in Oxborough et al. (2012) and tests if derived K_R measurements can be validated for any active fluorometer that has a defined excitation and emission detection spectrum, and has been accurately calibrated against a standard (i.e., chl a in 90% acetone) of known concentration, quantum yield of

Table 5. Equations used in the derivation of $a_{PSII}(\lambda)$

Eq.	Formula
Direct and "Fixed n_{PSII}" measures of a_{PSII}	
3)	$a_{PSII}(\lambda_{ex}) = [RCII] \cdot \sigma_{PSII}(\lambda_{ex}) \cdot 6.023\times10^5$
4)	$a_{PSII.npsii}(\lambda_{ex}) = 0.002 \cdot [chla] \cdot \sigma_{PSII}(\lambda_{ex}) \cdot 0.674$*
5)	$n_{PSII} = [RCII] \cdot [chla]^{-1} \cdot 8.925\times10^5$
Optical measures of a_{PSII}	
6)	$a_i(\lambda) = [c_i] \cdot a_i^*(\lambda)$
7)	$a_{sol}(\lambda) = \Sigma\left([c_i] \cdot a_i^*(\lambda)\right)$
8)	$Q_{abs}^*(\lambda) = a_\phi(\lambda) \cdot a_{sol}(\lambda)^{-1}$
9)	$a_{PS}(\lambda) = a_\phi(\lambda) - a_i(\lambda) \cdot Q_{abs}^*(\lambda)$**
10)	$a_{LHII}(\lambda) = F_{PSII}(\lambda) \cdot \left(\Sigma a_{PS}(\lambda)/\Sigma F_{PSII}(\lambda)\right) \cdot 0.5^\dagger$
11)	$a_{PSII.opt}(\lambda) = a_{LHII}(\lambda) \cdot \phi_{PSII}$
12)	$fAQ_{PSII}(\lambda_{ex}) = a_{PSII}(\lambda_{ex}) \cdot \left(a_{PS}(\lambda_{ex}) \cdot \phi_{PSII}\right)^{-1}$
13)	$fAQ_{PSII} = \frac{\Sigma F_{PSII}(\lambda) \cdot \Sigma a_{PS}(\lambda_{ex}) \cdot fAQ_{PSII}(\lambda_{ex})}{\Sigma a_{PS}(\lambda) \cdot \Sigma F_{PSII}(\lambda_{ex})}$
Fixed K_R measures of a_{PSII}	
14)	$\phi_f = k_f/(k_p + k_f + k_d)$
15)	$\phi_p = k_p/(k_p + k_f + k_d)$
16)	$F_0(\lambda_{EX}) \propto \phi_f \cdot a_{LHII}(\lambda_{EX}) \cdot E_{LED}(\lambda_{EX})$
17)	$F_0(\lambda_{EX}) \propto k_f/k_p \cdot a_{PSII}(\lambda_{ex}) \cdot E_{LED}(\lambda_{EX})$
18)	$F_0(\lambda_{EX}) = K_R^{-1} \cdot a_{PSII}(\lambda_{ex}) \cdot E_{LED}(\lambda_{EX})$
19)	$F_0^{std}(\lambda_{EX}) = K_R^{-1} \cdot a_{PSII}(\lambda_{ex})$
20)	$K_R = a_{PSII}(\lambda_{ex}) \cdot F_0^{std}(\lambda_{EX})^{-1}$
21)	$a_{PSII.Kr}(\lambda_{ex}) = F_0^{std}(\lambda_{EX}) \cdot K_R$
Approximation of K_{std} and $a_{PSII.std}(\lambda_{ex})$	
22)	$F_0(\lambda_{ex}) = E(\lambda) \cdot a_{LHII}(\lambda) \cdot \phi_f \cdot \Phi_F(\lambda_{em})$
23)	$F_0(\lambda_{ex}) = E(\lambda) \cdot a_{PSII}(\lambda_{ex}) \cdot k_f/k_p \cdot \Phi_F(\lambda_{em})$
24)	$K_{std} = a_{std}^*(\lambda_{ex}) \cdot \frac{\phi_f^{std}}{k_f/k_p} \cdot \frac{\Phi_F^{std}(\lambda_{em})}{\Phi_F(\lambda_{em})}$
25)	$a_{std}^*(\lambda_{ex}) = \frac{\int_{\lambda=400}^{\lambda=700} a_{std}^*(\lambda) \cdot E_{LED}(\lambda_{ex}) \cdot d\lambda}{\int_{\lambda=400}^{\lambda=700} E_{LED}(\lambda_{ex}) \cdot d\lambda}$
26)	$\Phi_F^{std}(\lambda_{em})/\Phi_F(\lambda_{em}) = \frac{\int F_{std} \cdot T_{em} \cdot PMT}{\int F_{PSII} \cdot T_{em} \cdot PMT}$

*0.002 represents assumed n_{PSII}.
**i denotes ppc and pheo.
†0.5 represents assumed fAQ_{PSII}.

fluorescence (ϕ_f^{std}), and pigment-specific absorption spectrum ($a_{std}^*(\lambda_{EX})$). This alternative derivation K_R is denoted K_{std}.

From first principles, $F_0(\lambda)$ is the product of $E(\lambda_{ex})$, $a_{LHII}(\lambda)$, the quantum yield of fluorescence (ϕ_f), and an instrument-specific function representing the spectral dependence of emission detection ($\Phi_F(\lambda_{em})$ Eq. 22, Huot and Babin 2010). As above, the substitution of functional ($a_{PSII}(\lambda_{ex}) \cdot \phi_p^{-1}$) for optical ($a_{LHII}(\lambda_{ex})$) absorption in Eq. 22 yields Eq. 23 that links $F_0(\lambda_{ex})$ and $a_{PSII}(\lambda_{ex})$ through the proportionality constant k_f/k_p. Now, consider that in this study $F_0(\lambda_{ex})$ is normalized to $E_{LED}(\lambda_{ex})$ such that resultant $F_0^{std}(\lambda_{ex})$ measurements are equivalent to [chl a_{std}]. As K_R scales fluorescence to absorption, simply multiplying $F_0^{std}(\lambda_{ex})$ by the standard's corresponding pigment-specific absorption spectrum ($a_{std}^*(\lambda_{ex})$) scales fluorescence to absorption. In other words, instead of normalizing fluorescence measurements to the known concentration of the standard, this approach normalizes fluorescence measurements to the known absorption of the standard. Critically, this scaling procedure is valid for routine measurements if and only if the $k_f/k_p \cdot \Phi_F(\lambda_{em})$ of a given water sample or phytoplankton culture is equivalent to $\phi_f^{std} \cdot \Phi_F^{std}(\lambda_{em})$ of the standard. As shown below the products of these parameters are not equivalent, therefore, K_{std} is defined as the product of $a_{std}^*(\lambda_{ex})$, $\phi_f^{std}/(k_f/k_p)$, and $\Phi_F^{std}(\lambda_{em})/\Phi_F(\lambda_{em})$ (Eq. 24).

In Eq. 24, $a_{std}^*(\lambda_{ex})$ can be estimated from a published or measured spectrum of chl *a* in 90% acetone and a measurement of the instrument's excitation spectrum ($E_{LED}(\lambda_{ex})$, Eq. 25). For chl *a* in 90% acetone, ϕ_f^{std} is taken as 0.30 (Huot and Babin 2010). Following Eqs. 14, 15, k_f/k_p is equivalent to ϕ_f/ϕ_p for photons absorbed by PSII pigments. As a first approximation, we estimate that $\phi_f/\phi_p = 0.10$ based on the mean probability of the different fates of absorbed photons as presented by Huot and Babin (2010). The ratio of emission detection of a chl *a* standard relative to a natural phytoplankton sample ($\Phi_F^{std}(\lambda_{em})/\Phi_F(\lambda_{em})$) was estimated following Eq. 26. This ratio is calculated as the spectral overlap of a chl *a* emission spectrum in 90% acetone ($F_{std}(\lambda_{em})$), the transmission spectrum of each FRRf's emission filter(s) ($T_{em}(\lambda)$), and the spectral response of each FRRf's photomultiplier tube (PMT(λ)), divided by the spectral overlap of an assumed PSII emission spectrum ($F_{PSII}(\lambda_{em})$), $T_{em}(\lambda)$ and PMT(λ). All spectra are shown in Fig. 1. $F_{std}(\lambda_{em})$ was measured on a scanning spectrofluorometer (Varian Cary Eclipse, Palo Alto), normalized to a wavelength-specific quantum correction factor following Kopf and Heinze (1984). $F_{PSII}(\lambda_{em})$ was approximated by a Gaussian distribution with a maximum peak at 683 nm and a half bandwidth of 25 nm (Collins et al. 1985). Table 1 lists the instrument-specific optical filters and PMT shown in Fig. 1. In the Assessment, K_{std} is derived for each instrument and compared to K_R.

Spectral correction factors

To compare $a_{PSII}(\lambda_{ex})$, $\sigma_{PSII}(\lambda_{ex})$, $F_0^{std}(\lambda_{ex})$, and E_K across instruments with different excitation and actinic spectra, spectral correction factors (SCFs) were derived to scale these measurements to a common reference spectrum. Spectrally scaled values are denoted $\bar{a}_{PSII}$, $\bar{\sigma}_{PSII}$, $\bar{F}_0^{std}$, and $\bar{E}_K$, respectively. SCFs for $a_{PSII}(\lambda_{ex})$ and $\sigma_{PSII}(\lambda_{ex})$ are dependent on $E_{LED}(\lambda_{ex})$ and $a_{LHII}(\lambda)$ for a given instrument and culture respectively, while SCFs for $F_0^{std}(\lambda_{ex})$ are also dependent on $a_{std}^*(\lambda_{ex})$. As an example, Fig. 2 shows $E_{LED}(\lambda_{ex})$ of a MKIII ($E_{MK3}(\lambda_{ex})$) and MKII $E_{MK2}(\lambda_{ex})$ FRRf, $a_{LHII}(\lambda)$ of *Thalassiosira pseudonana*, and $a_{std}^*(\lambda_{ex})$. For graphical clarity, $E_{MK3}(\lambda_{ex})$ and $E_{MK2}(\lambda_{ex})$ in Fig. 2 are normalized to unity, while the separate *y*-axis for $a_{LHII}(\lambda)$ and $a_{std}^*(\lambda_{ex})$ have been adjusted such

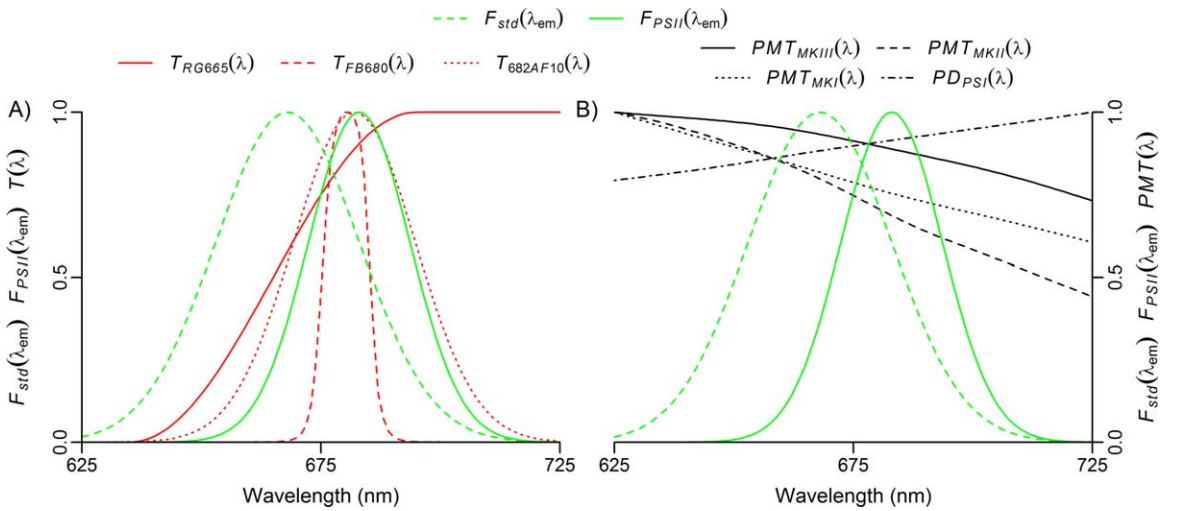

Fig. 1. Emission spectra of chl *a* in 90% acetone ($F_{std}(\lambda_{em})$) and PSII ($F_{PSII}(\lambda_{em})$) alongside (A) the transmission spectra and (B) spectral responses of the PMT and photodiode (PD) for the FRRfs used in this study (Table 1).

that the area under each curve is equivalent. Here, SCFs for $a_{PSII}(\lambda_{ex})$ and $\sigma_{PSII}(\lambda_{ex})$ scale each measurement to a flat spectrum, such that SCFs are derived as $a_{LHII}(\lambda)$ averaged across the PAR spectrum ($\hat{a}_{LHII}$) divided by $a_{LHII}(\lambda_{ex})$ (Eqs. 27, 28). Figure 2 illustrates that $E_{MK3}(\lambda_{ex})$ and $E_{MK2}(\lambda_{ex})$ each excite *T. pseudonana* in a region of comparatively high absorption, so that $a_{LHII}(\lambda_{ex})$ for both the MKIII ($0.19\,m^{-1}$) and MKII ($0.14\,m^{-1}$) exceed $\hat{a}_{LHII}$ ($0.11\,m^{-1}$). Consequently, *SCFs* for this culture decreases $a_{PSII}(\lambda_{ex})$ and $\sigma_{PSII}(\lambda_{ex})$ by a factor 0.52 (0.11/0.19) and 0.78 (0.11/0.14) for the MKIII and MKII respectively. As measurements of $F_0^{chl}(\lambda_{ex})$ in this study are expressed equivalent to [chl a_{std}], a second SCF (SCF_{std}) must be derived. SCF_{std} is calculated as the product of SCF and the ratio of $a^*_{std}(\lambda_{ex})$ to $\hat{a}^*_{std}$ (Eq. 29). In Fig. 2 the derived SCF_{std} for the MKIII and MKII instruments for *T. pseudonana* are 1.06 and 0.14, respectively. For the MKIII,

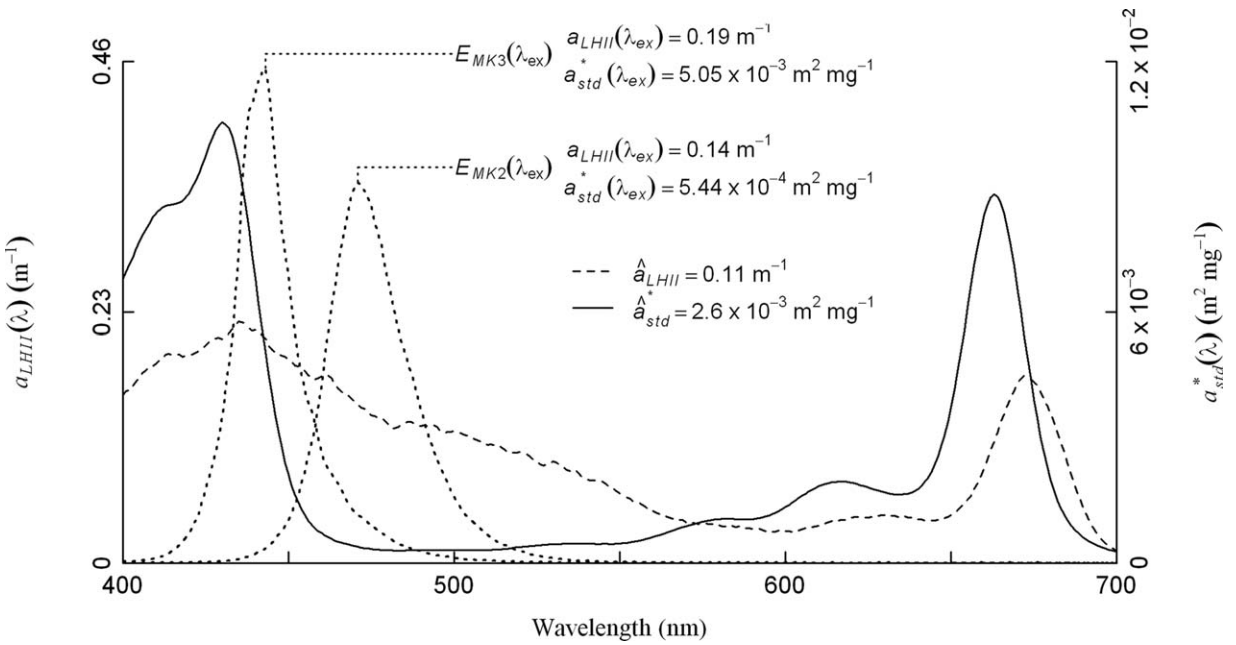

Fig. 2. Excitation spectra of a Chelsea MKIII ($E_{MK3}(\lambda_{ex})$) and MKII FRRF ($E_{MK2}(\lambda_{ex})$) are shown as dotted lines alongside the absorption spectrum of light-harvesting II pigments ($a_{LHII}(\lambda)$) of *Thalassiosira psuedonana* and $1\,mg\,m^{-3}$ of a chl *a* standard in 90% acetone ($a^*_{std}(\lambda)$). Next to each excitation spectrum label, the corresponding absorption coefficients weighted to $a_{LHII}(\lambda_{ex})$ and $a^*_{std}(\lambda_{ex})$ are shown. The mean $a_{LHII}(\lambda)$ and $a^*_{std}(\lambda)$ across the PAR spectrum ($\hat{a}_{LHII}$, $\hat{a}^*_{std}$) are stated for reference.

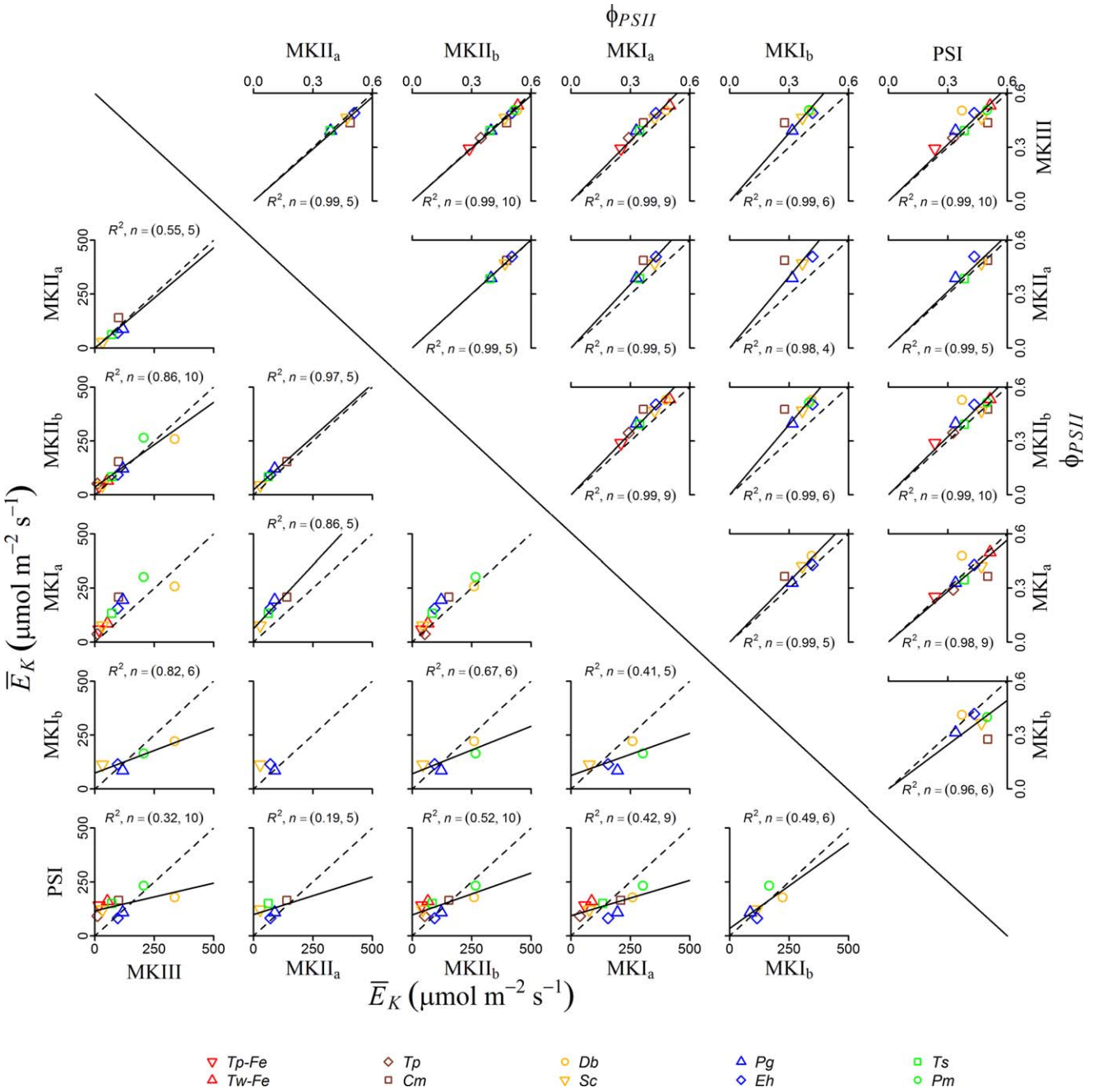

Fig. 3. Covariance matrices of ϕ_{PSII} and $\bar{E}_K$ derived from FLCs for each culture where FRRf instruments vary across panels. Dashed lines represent the line of equivalency and solid lines are the slopes of linear regressions for paired samples that are not significant different (Wilcoxon signed-rank test, $p > 0.05$).

the calculated SCF_{std} is close to unity because the spectral overlap of $E_{MK3}(\lambda_{ex})$ with $a_{LHII}(\lambda)$ and $a^*_{std}(\lambda)$ are approximately the same. For the MKII, the calculated SCF_{std} is small because the spectral overlap of $E_{MK2}(\lambda_{ex})$ with $a_{LHII}(\lambda)$ is much greater than the spectral overlap of $E_{MK2}(\lambda_{ex})$ with $a^*_{std}(\lambda)$. SCFs were also applied to FLC-derived E_K measurements because the actinitic irradiance spectra ($E(\lambda_{ac})$) varied across instruments. Here, each E_K value was multiplied by an instrument- and culture-specific SCF (SCF_{ac}, Eq. 30), where $a_{LHII}(\lambda_{ac})$ was derived from Eq. 31.

$$a_{LHII}(\lambda_{ex}) = \int_{400}^{700} a_{LHII}(\lambda) \cdot E_{LED}(\lambda_{ex}) \Big/ \int_{400}^{700} E_{LED}(\lambda_{ex}) \tag{27}$$

$$SCF = \hat{a}_{LHII} \cdot a_{LHII}(\lambda_{ex})^{-1} \tag{28}$$

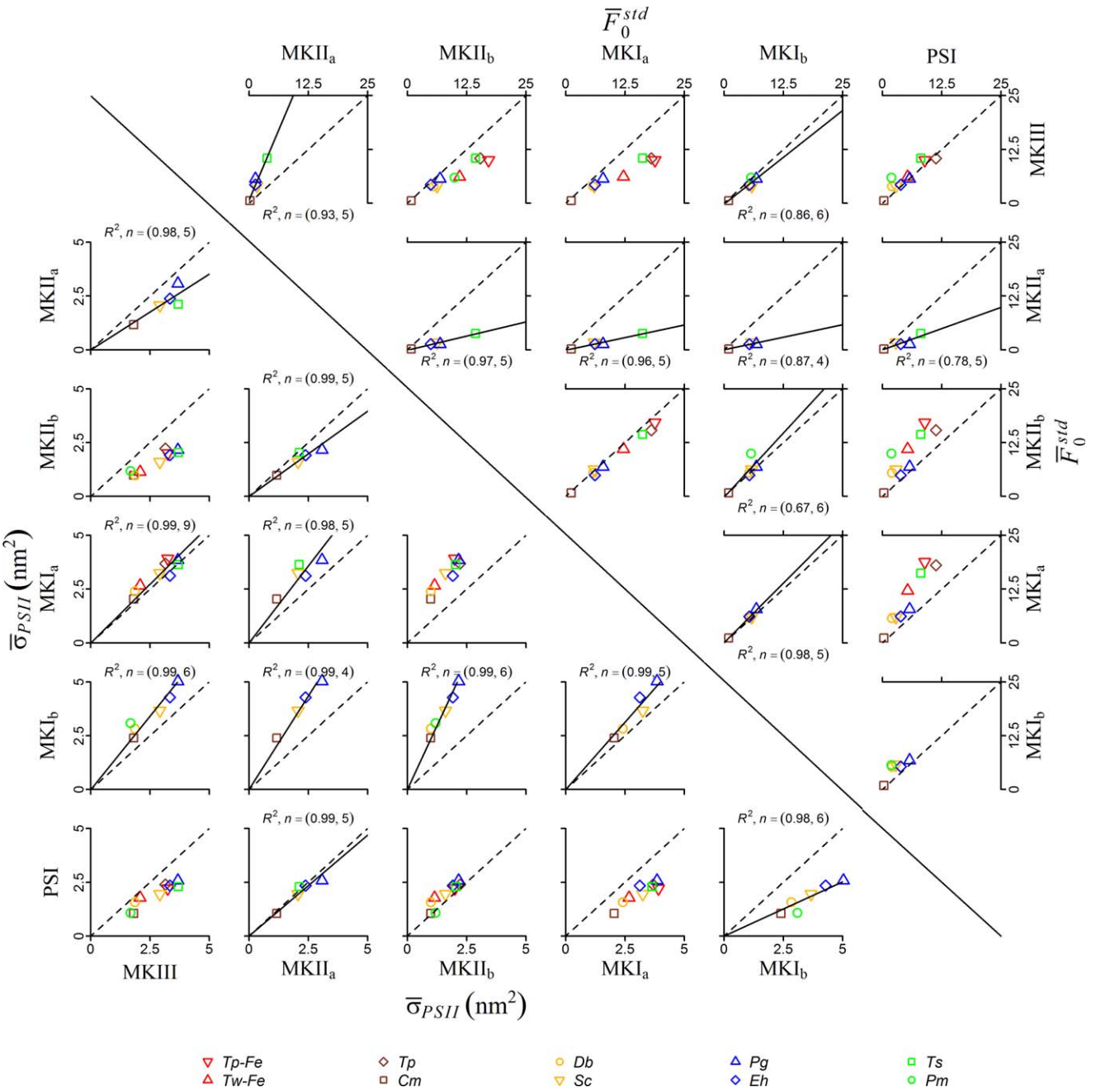

Fig. 4. Covariance matrices of $\bar{F}_0^{\mathrm{std}}$ and $\bar{\sigma}_{\mathrm{PSII}}$ culture measurements where FRRf instruments vary across panels. Dashed lines represent the line of equivalency and solid lines are the slopes of linear regressions for paired samples that are not significant different (Wilcoxon signed-rank test, $p > 0.05$).

$$\mathrm{SCF_{std}} = \mathrm{SCF} \cdot a^*_{\mathrm{std}}(\lambda_{\mathrm{ex}}) \cdot \hat{a}^{*\,-1}_{\mathrm{std}} \tag{29}$$

$$\mathrm{SCF_{ac}} = \hat{a}_{\mathrm{LHII}} \cdot a_{\mathrm{LHII}}(\lambda_{\mathrm{ac}})^{-1} \tag{30}$$

$$a_{\mathrm{LHII}}(\lambda_{\mathrm{ac}}) = \int_{400}^{700} \langle a_{\mathrm{LHII}}(\lambda) \cdot E(\lambda_{\mathrm{ac}}) \rangle \Big/ \int_{400}^{700} E(\lambda_{\mathrm{ac}}) \tag{31}$$

Assessment

FRRf intercalibration measurements

Measurements of ϕ_{PSII} and $\bar{E}_K$ made on parallel cultures across the six instruments are presented as covariance matrices in Fig. 3. Individual panels compare culture measurements made in parallel on two FRRfs. Comparisons of $\bar{F}_0^{\mathrm{std}}$ and $\bar{\sigma}_{\mathrm{PSII}}$ are similarly presented in Fig. 4. For each comparative dataset, a Wilcoxon signed-rank test is

used to test the null hypothesis that culture measurements are different between two instruments. As this nonparametric test compares relative ranking, it is insensitive to any consistent instrument bias that may arise from, for example, poor calibration. In each panel, the dashed line represents the line of equivalency while a solid line, if present, is a linear regression. Regression lines are only shown for measurement sets where the Wilcoxon signed-rank is not significantly different ($p > 0.05$), and the slopes of these lines tested if they are significantly different than the line of equivalency. As filtrate measurements did not exhibit any variable fluorescence (induction curves were flat), the linear regressions for ϕ_{PSII} and $\bar{\sigma}_{PSII}$ were forced through the origin.

Culture measurements of ϕ_{PSII} exhibited a high degree of correspondence across instruments. All 15 ϕ_{PSII} datasets (panels in Fig. 3) were not significantly different (Wilcoxon test, $p > 0.05$), and the fraction of variance explained by all linear regressions exceeded 0.96. Despite this high degree of covariance, some instrument-specific variability for ϕ_{PSII} measurements is apparent. The slopes of the linear regressions ranged from 0.82 to 1.32, with 5 of the 15 slopes significantly different than the line of equivalency ($p < 0.05$). These significant differences from the line of equivalency occurred between the newer (MKIII and MKII) and older (MKI) Chelsea FRRfs. The MKIII and MKII models yielded the highest ϕ_{PSII} measurements and were consistent between instruments, but on average exceeded ϕ_{PSII} measurements on the MKI models by a factor of 1.22. Measurements of ϕ_{PSII} made on the PSI FRRf generally fell in between the newer and older Chelsea instruments, and it is unclear why these instrument-specific discrepancies arise. With respect to $\bar{E}_K$, 12 of the 15 measurement sets were not significantly different (Wilcoxon test, $p > 0.05$). The fraction of variance explained by linear regressions for $\bar{E}_K$ ranged from 0.19 to 0.97, with the lowest values corresponding to the PSI instrument. The slopes of these regressions ranged from 0.33 to 1.18, of which 6 of the 15 slopes were not significantly different than the line of equivalency ($p < 0.05$). Across all instruments, the MKII and MKIII instruments yielded comparable $\bar{E}_K$ measurements. As FastAct systems with the same cool white actinic spectrum and light steps were used for all MKIII and MKII FLCs, it seems likely that some of the variability in $\bar{E}_K$ measurements may be an artefact of how the FLCs were performed. While the PSI FLCs were unique in that they were performed under a blue actinic spectrum, the application of spectral correction factors (Eq. 30) should compensate for different actinic light spectra. What is likely driving the diminished covariance between the $\bar{E}_K$ values measured on the PSI relative to the other FRRfs is the faster and variable duration of light steps (150–250 s) used for the PSI measurements. E_K is sensitive to FLC duration where faster light steps correspond to smaller E_K measurements (Ihnken et al. 2010), consistent with the PSI measurements shown in Fig. 3.

Measurements of $\bar{F}_0^{std}$ and $\bar{\sigma}_{PSII}$ also showed a high degree of correspondence across most instruments (Fig. 4). Of the 15 $\bar{F}_0^{std}$ datasets (panels in Fig. 4), 8 did not show significant differences between instruments (Wilcoxon test, $p > 0.05$). The fraction of variance explained by these 8 $\bar{F}_0^{std}$ linear regressions ranged from 0.67 to 0.97. Despite this high degree of covariance, instrument-specific variability for $\bar{F}_0^{std}$ measurements is apparent. The slopes of all 15 linear regressions ranged from 0.23 to 2.62, and the slope of 9 of 15 linear regressions were significantly different than the line of equivalency ($p > 0.05$). Had SCFs not been applied $\bar{F}_0^{std}$ measurements, the range of slopes would have increased to 0.07 to 4.22. With respect to $\bar{\sigma}_{PSII}$, 10 of the 15 measurement sets were not significantly different (Wilcoxon test, $p > 0.05$). Like $\bar{F}_0^{std}$, the linear regression slopes for $\bar{\sigma}_{PSII}$ measurements showed instrument-specific departures from the line of equivalency. Across all intercalibration $\bar{\sigma}_{PSII}$ measurement sets, the linear regression slopes were significantly different ($p > 0.05$) than the line of equivalency in 13 of 15 instances. The slopes of the linear regressions were smaller for $\bar{\sigma}_{PSII}$ than for $\bar{\sigma}_{PSII}$ slopes, ranging from 0.50 to 2.37, with a mean and standard deviation of 1.14 and 0.53, respectively. The largest departures from the line of equivalency correspond to $\bar{\sigma}_{PSII}$ measurements made on the MKI FRRfs.

Given the general high degree of correspondence between all instruments as shown by the Wilcoxon signed-rank test, the departure of the linear regressions from the line of equivalency in Figs. 3 and 4 are largely independent of phytoplankton taxa. For example, across all instruments specific cultures (*Cm, Pm, Tp*) consistently yielded the lowest measures of $\bar{\sigma}_{PSII}$ while other cultures (*Eh, Pg, Ts*) consistently yielded the highest measures of $\bar{\sigma}_{PSII}$. Figure 4 also shows a consistent culture-dependent ranking of $\bar{F}_0^{std}$ measurements across instruments as was also observed with measurements of ϕ_{PSII} and p (data not shown). Instrument-specific differences in fluorescence measurements are also not likely the result of the different fitting algorithms applied to the single-turnover induction curves, as noted in Materials and Procedures. Instead the two most likely sources for the lack of correspondence were: (i) Any measurement errors in $E_{LED}(\lambda_{ex})$ or $F_{PSII}(\lambda_{ex})$ that would then propagate through to the SCFs used to scale $F_0^{std}(\lambda_{ex})$ and $\sigma_{PSII}(\lambda_{ex})$ (Fig. 1; Eqs. 27, 29) or (ii) inaccurate calibration coefficients or an instrument-specific deviation from its respective calibration due to, for example, optical fouling. For example, determination of $\sigma_{PSII}(\lambda_{ex})$ is dependent on a precise measure of $E_{LED}(\lambda_{ex})$. During calibration $E_{LED}(\lambda_{ex})$ is measured with a PAR sensor positioned at the intersection of the illuminated and observed volume. With the Mk II and FastOcean sensors, computer modeling was used to generate an optical arrangement that provides very even illumination throughout a 1 cm^3 volume, and collection optics that maximize the collection of fluorescence generated within this volume. The Mk I was not modeled in this way. One practical issue with the Mk I is that the radiometer specifically designed for

Table 6. Direct, "fixed n_{PSII}" and optical measures of $a_{PSII}(\lambda)$ and their constituent variables. [RCII], $\sigma_{PSII}(\lambda_{ex})$, and ϕ_{PSII} values are the mean ± the standard error. $\sigma_{PSII}(\lambda_{ex})$ are from the MKIII FRRf, therefore $a_{PSII}(\lambda)$ measurements in this table are specific to this instrument

Culture	[RCII] (nmol m^{-3})	[chl *a*] (mg m^{-3})	n_{PSII} (mol RCII/mol chl *a*)	$\sigma_{PSII}(\lambda_{ex})$ (nm^{-2})	$a_{PSII}(\lambda_{ex})$ (m^{-1})	$a_{PSII.npsii}(\lambda_{ex})$ (m^{-1})
Tp-Fe	22.6±1.3	33.3	6.06×10^{-4}	6.15±0.03	8.36×10^{-2}	2.76×10^{-1}
Tw-Fe	28.6±1.0	25.6	9.97×10^{-4}	3.77±0.01	6.50×10^{-2}	1.30×10^{-1}
Tp	34.5±1.4	39.9	7.72×10^{-4}	6.06±0.04	1.26×10^{-1}	3.27×10^{-1}
Cm	2.90±0.1	2.7	9.59×10^{-4}	3.32±0.03	5.80×10^{-3}	1.21×10^{-2}
Db	22.8±0.6	22.6	8.99×10^{-4}	3.19±0.02	4.37×10^{-2}	9.73×10^{-2}
Sc	13.2±0.4	13.6	8.69×10^{-4}	4.75±0.03	3.79×10^{-2}	8.72×10^{-2}
Pg	16.3±0.4	13.9	1.04×10^{-3}	6.63±0.04	6.50×10^{-2}	1.25×10^{-1}
Eh	11.5±0.6	8.0	1.29×10^{-3}	6.61±0.04	4.56×10^{-2}	7.10×10^{-2}
Ts	33.9±0.9	23.9	1.27×10^{-3}	5.46±0.02	1.12×10^{-1}	1.76×10^{-1}
Pm	34.4±1.1	22.3	1.38×10^{-3}	3.09±0.01	6.41×10^{-2}	0.93×10^{-2}

measuring $E_{LED}(\lambda_{ex})$ is collecting photons from a larger volume than the PMT is seeing fluorescence from. The end result is that the PMT-dependent $E_{LED}(\lambda_{ex})$ value is higher than the number provided on the calibration certificate and the calculated values of $\sigma_{PSII}(\lambda_{ex})$ are (as a consequence) also greater than what they should be. This is indeed consistent with the data shown in Fig. 4 where the MK1 fluorometers yielded the largest $\bar{\sigma}_{PSII}$ measurements. In this study, measurements of $F_0^{std}(\lambda_{ex})$ have been normalized against [chl a_{std}] with resultant values expressed in [chl a_{std}] equivalency. Any error in the calibration coefficient(s) used to normalize $F_0^{std}(\lambda_{ex})$ (Supporting Information) can explain consistent instrument biases shown in Fig. 4. For example, across all cultures the $MKII_a$ and $MKII_b$ FRRfs consistently reported the smallest and largest $\bar{F}_0^{std}$ measurements, respectively.

Methods evaluation of $a_{PSII}(\lambda)$

Direct and "fixed n_{PSII}" measures of $a_{PSII}(\lambda)$

Table 6 tabulates $a_{PSII}(\lambda_{ex})$ and $a_{PSII.npsii}(\lambda_{ex})$ measurements including their constituent data; $a_{PSII}(\lambda_{ex})$ is the

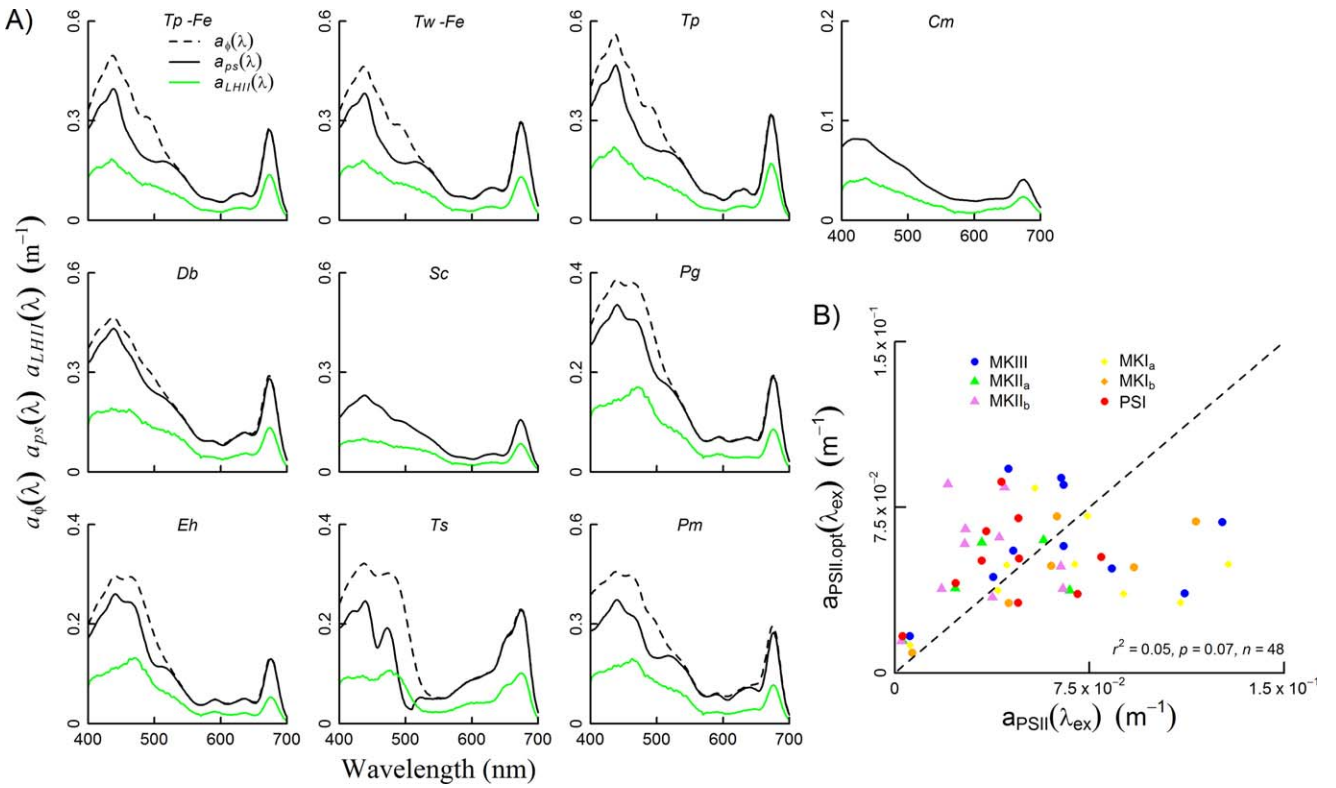

Fig. 5. A: Absorption coefficient of phytoplankton pigments ($a_\phi(\lambda)$), photosynthetic pigments ($a_{ps}(\lambda)$), and light-harvesting II pigments ($a_{LHII}(\lambda)$) of the 10 phytoplankton taxa investigated. B: Covariance of $a_{PSII}(\lambda_{ex})$ and $a_{PSII.opt}(\lambda_{ex})$ across cultures and instruments.

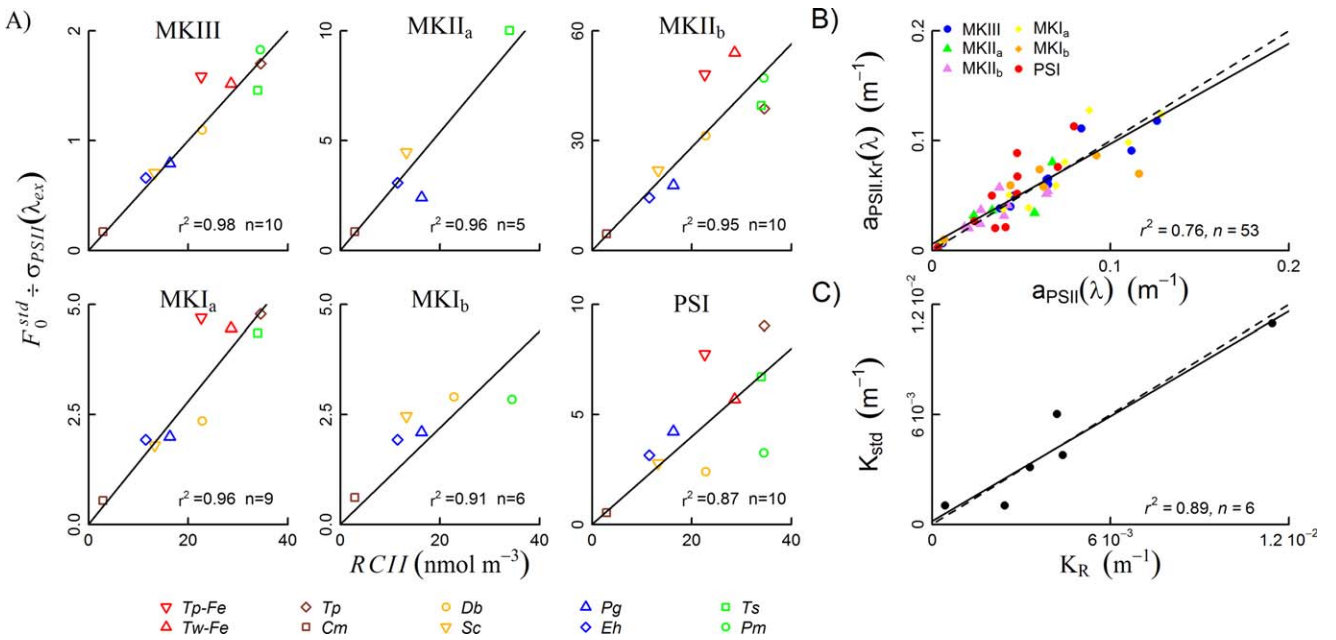

Fig. 6. A: RCII concentrations vs. $F_0^{std}/\sigma_{PSII}(\lambda_{ex})$ for each culture across six FRRFs. B: Covariance of $a_{PSII}(\lambda_{ex})$ and $a_{PSII.Kr}(\lambda_{ex})$ across cultures and instruments. C: Comparison of K_R and K_{std} for the six FRRfs. In (B) and (C) the dashed line represents equivalency and the solid line is the linear regression.

product of [RCII] and $\sigma_{PSII}(\lambda_{ex})$ (Eq. 3), while $a_{PSII.npsii}(\lambda_{ex})$ is the product of [chl *a*], an assumed n_{PSII} value of 2×10^{-3} mol RCII (mol chl *a*)$^{-1}$, and $\sigma_{PSII}(\lambda_{ex})$ (Eq. 4). As both methods are dependent on instrument-specific $\sigma_{PSII}(\lambda_{ex})$ values, data presented in Table 6 correspond to the MKIII FRRf. Measurements of [RCII] and [chl *a*] permit the derivation of n_{PSII} (Eq. 5), these values are also presented in Table 6 for each culture. All cultures had n_{PSII} values lower than 2×10^{-3} mol RCII (mol chl *a*)$^{-1}$, and consequently $a_{PSII.npsii}(\lambda_{ex})$ overestimated $a_{PSII}(\lambda_{ex})$ by a factor of 1.45 to 3.30. That said, the covariation between $a_{PSII}(\lambda_{ex})$ and $a_{PSII.npsii}(\lambda_{ex})$ was significant across all cultures and instruments ($r^2 = 0.82$, $p < 0.05$, $n = 48$), although the slope of the linear regression was 2.28. Of all cultures, the two diatoms grown in iron-deplete media had among the lowest n_{PSII} values, which is consistent with literature (Greene et al. 1991; Geider et al. 1993).

Optical measures of $a_{PSII}(\lambda)$

Figure 5A shows $a_\phi(\lambda)$ as measured with the PSICAM, $a_{PS}(\lambda)$ derived as $a_\phi(\lambda) - a_{NP}(\lambda)$ (Eq. 9), and $a_{LHII}(\lambda)$ derived by scaling $F_{PSII}(\lambda)$ to $a_{PS}(\lambda)$ assuming fAQ_{PSII} is 0.5 across the PAR spectrum (Eq. 10). For the 8 cultures where HPLC measures of photoprotective carotenoids were available, $a_{NP}(\lambda)$ accounted for as little as 8% of $a_\phi(\lambda)$ in *Ditylum brightwellii* but as much as 27% of $a_\phi(\lambda)$ for *Tetraselmis striata*. Figure 5B compares optical $a_{PSII.opt}(\lambda_{ex})$ measurements (Eq. 11) to direct $a_{PSII}(\lambda_{ex})$ estimates (Eq. 3) across all cultures and FRRfs. In Fig. 5B, all measurements are spectrally confined to the excitation spectrum (λ_{ex}) of the stated FRRf. Across all instruments and cultures $a_{PSII}(\lambda_{ex})$ and $a_{PSII.opt}(\lambda_{ex})$ did not covary ($p = 0.07$, $n = 48$). The lack of covariation seems to be largely driven by taxa: Certain cultures consistently exceeded fAQ_{PSII} values of 0.5, while other cultures consistently had values below 0.5. For example, the two cultures where [ppc] was not measured (and

Table 7. Instrument specific K_R (mean ± standard error) and K_{std} values

Instrument	K_R (m^{-1}) All cultures	K_R (m^{-1}) Without -Fe Cultures	K_{std} (m^{-1})	$K_R \cdot K_{std}^{-1}$
MKIII	$1.14\times10^{-2}\pm4.68\times10^{-4}$	$1.18\times10^{-2}\pm4.33\times10^{-4}$	1.10×10^{-2}	1.04
MKII$_a$*	$2.44\times10^{-3}\pm4.17\times10^{-4}$	$2.44\times10^{-3}\pm4.17\times10^{-4}$	1.04×10^{-3}	2.35
MKII$_b$	$4.31\times10^{-4}\pm2.95\times10^{-5}$	$4.64\times10^{-4}\pm0.25\times10^{-5}$	1.04×10^{-3}	0.42
MKI$_a$	$4.19\times10^{-3}\pm3.03\times10^{-4}$	$4.43\times10^{-3}\pm3.24\times10^{-4}$	6.05×10^{-3}	0.69
MKI$_b$*	$4.39\times10^{-3}\pm4.79\times10^{-4}$	$4.39\times10^{-3}\pm3.16\times10^{-4}$	3.80×10^{-3}	1.15
PSI	$3.23\times10^{-3}\pm4.8\times10^{-4}$	$3.51\times10^{-3}\pm5.69\times10^{-4}$	3.14×10^{-3}	1.05

*Indicates instrument where K_R measures do not include *Tp-Fe* and *Tw-Fe* cultures.

consequently $a_{NP}(\lambda)$ was assumed to be 0), the mean ± standard deviation of calculated fAQ_{PSII} was 0.28 ± 0.17. The highest culture-specific mean fAQ_{PSII} values across cultures corresponded to *Tp-Fe* and *Tw-Fe* (0.83 and 0.90, respectively). These extreme values are consistent with very high PSII : PSI ratios in iron-limited diatoms that arise due to the increased Fe content of PSI complexes (Strzepek and Harrison 2004).

Absorption (K_R) based measures of $a_{PSII}(\lambda)$

Figure 6A illustrates the covariance between FRRf measurements of $F_0^{std} \times {\sigma_{PSII}}^{-1}$ and the flash yield derived measurements of [RCII]. The slopes of the linear regressions are proportional to K_R (Eq. 18), and the mean and standard error of K_R across cultures is presented in Table 7 for each instrument. The variance in $F_0^{chl} \times {\sigma_{PSII}}^{-1}$ explained by [RCII] ranged from 0.86 to 0.98 across FRRfs. Accordingly K_R variance is muted for each instrument (Table 7). Instrument-specific mean K_R values spanned two orders of magnitude ranging from $4.31 \times 10^{-4}\,m^{-1}$ to $1.14 \times 10^{-2}\,m^{-1}$. Figure 6A also illustrates that specific cultures routinely yielded K_R estimates both above and below instrumental mean K_R values. With the exception of *Tw-Fe* measured on the PSI fluorometer, both *Tp-Fe* and *Tw-Fe* cultures grown in the absence of iron predicted higher [RCII] than measured. Consequently these cultures yielded lower K_R values than other cultures. This key finding is consistent with the concept that iron-limited phytoplankton may accumulate a store of nonenergetically coupled chlorophyll-binding complexes that increases the quantum yield of fluorescence (ϕ_f) relative to iron replete phytoplankton (Behrenfeld and Milligan 2013; Macey et al. 2014). As K_R is proportional to ϕ_P/ϕ_f, an increase in ϕ_f would diminish K_R as observed in this study. Omission of these iron-deplete cultures generally increased the mean K_R value for each instrument and reduced its variance (Table 7). The largest departure between an instrument-specific mean K_R value and a single K_R value corresponds to the *Pm* culture measured on the PSI FRRf, where the culture-specific K_R value was 1.93 greater than the instrument mean. This instrument $E_{LED}(\lambda_{ex})$ settings for this culture on the PSI FRRf was twice that of all other culture measurements, so it possible that a calibration error is in part driving the departure from the instrument-specific mean K_R value. Figure 6B compares direct measures of $a_{PSII}(\lambda_{ex})$ (Eq. 3) with $a_{PSII.Kr}(\lambda)$ (Eq. 21). As above, each data point presented in Fig. 6B is spectrally confined to λ_{ex} of the stated FRRf. Across all measurements and instruments, the covariance of $a_{PSII}(\lambda_{ex})$ and $a_{PSII.Kr}(\lambda_{ex})$ was statistically significant ($r^2 = 0.76$, $p < 0.01$, $n = 53$), and the slope and intercept were not significantly different than 1 and 0, respectively ($p < 0.05$). The strong covariation and linear regression near the line of equivalency shown in Fig. 6B is not surprising given the strong covariance shown in Fig. 6A but also because $a_{PSII.Kr}(\lambda_{ex})$ is inherently scaled to $a_{PSII}(\lambda_{ex})$.

Table 7 also lists K_{std} values derived from instrument-specific [chl a_{std}] calibration measures and optical configurations (Eq. 24). A linear regression of measured K_R vs. K_{std} was statistically significant ($r^2 = 0.89$, $p < 0.01$, $n = 6$, Fig. 6C). As shown in Table 7, K_{std} was within 15% of the measured K_R for three instruments (MKIII, MKI_b, and PSI). Recall that across fluorometers, the $MKII_a$ and $MKII_b$ yielded the lowest and highest measures of $\bar{F}_0^{std}$, respectively (Fig. 4). Consistent with this discrepancy, the $MKII_a$ and $MKII_b$ also yielded the lowest and highest measures of $K_R \cdot {K_{std}}^{-1}$ (Table 7). Thus, it is plausible that either errors during the [chl a_{std}] calibration of these specific instruments or optical fouling not only caused $\bar{F}_0^{std}$ intercalibration measures to depart from the line of equivalency, but also may be responsible for the discrepancy between measured K_R and K_{std} calculated using [chl a_{std}] calibration data.

Discussion

FRRf intercalibration measurements

Measurements of ϕ_{PSII} and $\phi'_{PSII}(E)$ (represented here as $\bar{E}_K$) showed a high degree of correspondence across cultures and instruments, although some instrument-dependent biases were apparent. While the variability in $\bar{E}_K$ measurements across instruments was likely an artefact of how the FLCs were performed, the MKI FRRfs consistently yielded ϕ_{PSII} measurements lower than all other instruments. As we cannot identify the source of this discrepancy, it is not clear whether or not this is an artefact of all MKI FRRfs or specific to the two instruments in this study. That said as both our derivation of P_e in Eq. 2 and most P_e derivations in the literature (Lawrenz et al. 2013) are not dependent on the absolute magnitude of ϕ_{PSII} but rather the shape of its light response ($\phi'_{PSII}(E)/\phi_{PSII}$), this artefact does not affect the vast majority of past P_e measurements, and by extension past $\Phi_{e,C}$ measurements.

Fluorescence σ_{PSII} measurements across cultures generally displayed a high degree of correspondence, however, observed biases between instruments, shown in Fig. 4 as departures from the line of equivalency, raises important questions concerning instrument intercomparability. Unlike the instrument-specific ϕ_{PSII} discrepancies, our assessment has identified a mechanistic source for this variability that suggests historic σ_{PSII} measurements on MKI FRRfs have been overestimated. This has important implications as the vast majority of $\Phi_{e,C}$ data derived with paired P_e and P_C in the literature has computed P_e using $a_{PSII.npsii}(\lambda_{ex})$ that is dependent on $\sigma_{PSII}(\lambda_{ex})$ (Lawrenz et al. 2013). Consequently, an overestimation in σ_{PSII} will lead to proportional overestimations in both P_e and $\Phi_{e,C}$ in those studies that have used the $a_{PSII.npsii}(\lambda_{ex})$ formulation. Thus, it is plausible that the range of $\Phi_{e,C}$ measurements reported in studies using the MKI may be overestimated. As a growing number of FRRfs that have previously been used to measure $\Phi_{e,C}$ now have K_R values, recalculating past P_e measurements with $a_{PSII.Kr}(\lambda_{ex})$ may lead to more constrained $\Phi_{e,C}$ values.

Methods evalulation of $a_{PSII}(\lambda)$

With the exception of direct $a_{PSII}(\lambda)$ measurements calculated from paired [RCII] (oxygen flash yield) and σ_{PSII}

measurements, the accuracy and precision of $a_{PSII}(\lambda)$ across methods is largely determined by the variance of method-specific coefficients (n_{PSII}, fAQ_{PSII}, K_R). In this study, n_{PSII} calculated from paired [RCII] and [chl *a*] measurements were lower by a factor of 0.30–0.69 (Table 6) than the nominally assumed value of 2.00×10^{-3} mol RCII (mol chl *a*)$^{-1}$. Pooling n_{PSII} measurements from the literature that span a broad range of taxa and physiological conditions (Falkowski et al. 1981; Dubinsky et al. 1986; Greene et al. 1991; Suggett et al. 2004, 2006, 2009) yields a combined mean and coefficient of variance of 1.86×10^{-3} mol RCII (mol chl *a*)$^{-1}$ and 38%, respectively ($n = 69$). The range of n_{PSII} measurements from these combined studies vary by a factor of 0.46–2.12 about 2.00×10^{-3} mol RCII (mol chl *a*)$^{-1}$.

A second assumed parameter, fAQ_{PSII}, was calculated in this study to have a combined mean and coefficient of variance of 0.55 and 53%, respectively, not including the two cultures where [ppc] were not measured. The only dataset in the literature that calculates fAQ_{PSII} (through parallel direct and optical measures of $a_{PSII}(\lambda)$) is Suggett et al. (2004). In their study, fAQ_{PSII} had a combined mean and coefficient of variance of 0.46 and 23%, respectively ($n = 22$). Again, this data set was taken from a range of phytoplankton taxa and growth conditions but even so the range for fAQ_{PSII} (0.25–0.58) corresponds to a factor of 0.50–1.16 from the typical assumed value of 0.5.

Finally, Oxborough et al. (2012) present K_R measurements from a field-based study ($n = 19$) and from cultures ($n = 38$). The coefficient of variance for the field-based K_R measurements was 20% and ranged by a factor of 0.67–1.31 from the mean K_R value. The coefficient of variance for the culture-based measurements was 17% and ranged by a factor of 0.67–1.33 about the mean K_R value. In this study (Fig. 6B), that included iron-limited phytoplankton, the coefficient of variance of K_R is 29% with values ranging by a factor of 0.54–1.93 from the mean.

The variance of n_{PSII}, fAQ_{PSII}, K_R in this study as well as data pooled from the literature supports the application of an instrument-specific calibration coefficient (K_R) as the most accurate method to estimate a_{PSII}. Moreover, data from three of the six fluorometers in this study suggests that K_R can be approximated to within 15% from an active fluorometer that is accurately calibrated against a standard whose absorption spectrum and quantum efficiency are known (i.e., chl *a* in 90% acetone) through the derivation of K_{std}. The derivation of K_{std} presented here demonstrates that K_R invariance is not only dependent on invariance in the proportionality constant (k_f/k_p) as stated by Oxborough et al. (2012) but is also dependent on (1) accurate normalization of $F_0(\lambda_{ex})$ across instrument settings (photomultiplier gain, photon output of excitation light) and (2) consistent fluorescence emission, including the manner in which the sample is measured (e.g., cuvettes, flow-caps). The two instruments that yielded the lowest and highest measures of $\bar{F}_0^{std}$ (Fig. 4) also yielded the lowest and highest measures of $K_R \cdot K_{std}{}^{-1}$, respectively (Table 7). Thus, it is plausible that errors during the [chl a_{std}] calibration of these specific instruments not only caused $\bar{F}_0^{std}$ intercalibration measures to depart from the line of equivalency, but may also be responsible for the discrepancy between K_R and K_{std} for these two instruments.

Conclusions and recommendations

The assessment and discussion presented here firmly support the application of an instrument-specific calibration coefficient (K_R) as the most accurate method to estimate a_{PSII}. That said, direct measures of $a_{PSII}(\lambda_{ex})$ across diverse marine environments including nitrogen and iron-limited regions would help further confirm the invariance of K_R shown here in culture, and previously shown in two contrasting marine environments as well as cultures grown at different light levels (Oxborough et al. 2012). As FRRf-based fluorometry is currently the only methodology that permits P_e measurements from a single instrument (but see Schreiber et al. 2012), the K_R approach is best suited to capture photosynthetic variability through space and time. While this methodology represents an important step towards unattended deployments, we note that measures must be taken to include background fluorescence measurements ($F_{CDOM}(\lambda)$). The importance of $F_{CDOM}(\lambda)$ contamination is well known and can dramatically alter apparent ϕ'_{PSII} diurnal periodicity (Cullen and Davis 2004). Because K_R directly scales $F_0^{std}(\lambda_{ex})$ to $a_{PSII}(\lambda_{ex})$, failure to account for $F_{CDOM}(\lambda)$ will overestimate $a_{PSII}(\lambda_{ex})$. For studies or programs that seek accurate unattended photosynthetic measurements, $F_{CDOM}(\lambda)$ measurements are critical.

Our evaluation has underscored the utility and potential value of accurately calibrating instruments to a standard whose excitation spectrum and quantum yield is known (e.g., chl *a* in 90% acetone and additional fluorophores suitable for excitation bands of specific instruments). While most commercial manufacturers perform such calibrations, manufacturers and end users alike should ensure calibrations are performed as accurately as possible. Indeed it seems likely that some of the inter-instrument variability reported in this study is partially a result of inaccurate calibrations. To this end, we recommend that active fluorescence manufacturers provide end users detailed calibration protocols. In comparing FRRf-based photobiological parameters derived from various FRR fluorometers, and in turn their application to calculate $a_{PSII}(\lambda)$, we have provided the first means by which users can confidently and robustly reconcile absolute determinations of P_e; such an evaluation is an essential step towards wider implementation of active fluorometry to limnological and oceanographic studies.

References

Behrenfeld, M. J., and A. J. Milligan. 2013. Photophysiological expressions of iron stress in phytoplankton. Annu. Rev. Mar. Sci. **5**: 217–246. doi: 10.1890/09-1207.1

Behrenfeld, M. J., K. Worthington, R. M. Sherrell, F. P. Chavez, P. Strutton, M. McPhaden, and D. M. Shea. 2006. Controls on tropical Pacific Ocean productivity revealed through nutrient stress diagnostics. Nature **443**: 1025–1028. doi: 10.1038/nature05083

Bidigare, R. R., M. E. Ondrusek, J. H. Morrow, and D. A. Kiefer. 1990. In vivo absorption properties of algal pigments. Proc. SPIE. **1302**: 290–302. doi: 10.1117/12.21451

Bricaud, A., H. Claustre, J. Ras, and K. Oubelkheir. 2004. Natural variability of phytoplankton absorption in oceanic waters: Influence of the size structure of algal populations. J. Geophys. Res. **109**: C11010. doi: 10.1029/2004JC002419

Claustre, H., and others. 2010. Guidelines towards an integrated ocean observation system for ecosystems and biogeochemical cycles. *In* J. Hall, D. E. Harrison, and D. Stammer [eds.], Proceedings of OceanObs'09: Sustained Ocean Observations and Information for Society. ESA Publication WPP-306. doi: 10.5270/OceanObs09.pp14

Collins, D. J., D. A. Kiefer, J. B. Soohoo, and I. S. McDermid. 1985. The role of reabsorption in the spectral distribution of phytoplankton fluorescence. Deep-Sea Res. **32**: 983–1003. doi: 10.1016/0198-0149(85)90040-8

Cullen, J. J., and R. F. Davis. 2004. The blank can make a big difference in oceanographic measurements. Limnol. Oceanogr. Bull. **12**: 29–35. doi: 10.1002/lob.200413229

Dubinsky, Z., P. G. Falkowksi, and K. Wyman. 1986. Light harvesting and utilisation by phytoplankton. Plant Cell Physiol. **27**: 1335–1349.

European Marine Board. 2013. Navigating the Future IV. Position paper 20 of the European Marine Board. Ostend, Belgium.

Falkowski, P. G., T. G. Owens, A. C. Ley, and D. C. Mauzerall. 1981. Effects of growth irradiance levels on the ratio of reaction centers in two species of marine phytoplankton. Plant Physiol. **68**: 969–973. doi: 10.1104/pp.68.4.969

Geider, R. J., J. La Roche, R. M. Greene, and M. Olaizola. 1993. Response of the photosynthetic apparatus of Phaeodactylum tricornutum (Bacillariophycaea) to nitrate, phosphate, or iron starvation. J. Phycol. **29**: 755–766. doi: 10.1111/j.0022-3646.1993.00755.x

Gilbert, M., A. Becker, and C. Wilhelm. 2000. Estimation of primary productivity by chlorophyll *a in vivo* fluorescence in freshwater phytoplankton. Photosynthetica **38**: 111–126. doi: 10.1023/A:1026708327185

Greene, R. M, R. J. Geider, and P. G. Falkowksi. 1991. Effect of iron limitation on photosynthesis in a marine diatom. Limnol. Oceanogr. **36**: 1772–1782. doi: 10.4319/lo.1991.36.8.1772

Hartig, P., K. Wolfstein, S. Lippemeier, and F. Colijn. 1998. Photosynthetic activity of natural microphytobenthos populations measured by fluorescence (PAM) and 14C-tracer methods: A comparison. Mar. Ecol. Prog. Ser. **166**: 53–62. doi: 10.3354/meps166053

Huot, Y., and M. Babin. 2010. Overview of fluorescence protocols: Theory, basic concepts, and practice, p. 31–74. *In* D. J. Suggett, O. Prasil, and M. A. Borowitzka [eds.], Chlorophyll *a* fluorescence in aquatic sciences: Methods and applications. Springer.

Ihnken, S., A. Eggert, and J. Beardall. 2010. Exposure times affect photosynthetic parameters in algae. Aquat. Bot. **93**: 183–193. doi: 10.1016/j.aquabot.2010.07.002

Johnsen, G., and E. Sakshaug. 2007. Bio-optical characteristics of PSII and PSI in 33 species (13 pigment groups) of marine phytoplankton, and the relevance for pulse amplitude-modulated and fast repetition rate fluorometry. J. Phycol. **48**: 1236–1251. doi: 10.1111/j.1529-8817.2007.00422.x

Kolber, Z., and P. G. Falkowski. 1993. Use of active fluorescence to estimate photoplankton photosynthesis in situ. Limnol. Oceanogr. **38**: 1646–1665. doi: 10.4319/lo.1993.38.8.1646

Kolber, Z. S., O. Prášil, and P. G. Falkowski. 1998. Measurements of variable chlorophyll fluorescence using fast repetition rate techniques: Defining methodology and experimental protocols. Biochim. Biophys. Acta **1367**: 88–106. doi: 10.1016/S0005-2728(98)000135-2

Kopf, U., and J. Heinze. 1984. 2,7-Bis(diethyleamino)phenazoxonium chloride as a quantum counter for emission measurements between 240 and 700 nm. Anal. Chem. **56**: 1931–1935. doi: 10.1021/ac00275a039

Kromkamp, J., N. A. Dijkam, J. Peene, S. G. H. Simis, and H. J. Gons. 2008. Estimating phytoplankton primary production in Lake IJsselmeer (The Netherlands) using variable florescence (PAM-FRRF) and C-uptake techniques. Eur. J. Phycol. **43**: 327–344. doi: 10.1080/09670260802080895

Laney, S. R., and R. M. Letelier. 2008. Artifacts in measurements of chlorophyll fluorescence transients, with specific application to fast repetition rate fluorometry. Limnol. Oceanogr. Methods. **6**: 40–50. doi: 10.4319/lom.2008.6.40

Lawrenz, E., and others. 2013. Predicting the electron requirement for carbon fixation in seas and oceans. PLos One **8**: e58137. doi: 10.1371/journal.pone.0058137

Macey, A. I., T. Ryan-Keogh, S. Richier, C. M. Moore, and T. S. Bibby. 2014. Photosynthetic protein stoichiometry and photophysiology in the high latitude North Altantic. Limnol. Oceanogr. **59**: 1853–1864. doi: 10.4319/lo.2014.59.6.1853

Mauzerall, D., and N. L. Greenbaum. 1989. The absolute size of a photosynthetic unit. Biochim. Biophys. Acta. **974**: 119–140. doi: 10.1016/S0005-2728(89)80365-2

Mitchell, B. G. 1990. Algorithms for determining the absorption coefficient for aquatic particles using the quantitative filter technique. Proc. SPIE. **137**: 1302. doi: 10.1117/12.21440

Moore, C., A. Barnard, P. Fietzek, M. R. Lewis, H. M. Sosik, S. White, and O. Zielinski. 2008a. Optical tools for ocean monitoring and research. Ocean Sci. Discuss. **5**: 659–717. doi: 10.5194/os-5-661-2009

Moore, C. M., M. M. Mills, R. Langlois, A. Milne, E. P. Acterberg, J. La Roche, and R. J. Geider. 2008b. Relative

influence of nitrogen and phosphorus availability on phytoplankton physiology and productivity in the oligotrophic sub-tropical North Altantic Ocean. Limnol. Oceanogr. **53**: 291–305. doi: 10.4319/lo.2008.53.1.0291

Moore, C.M., and others. 2006. Phytoplankton photoacclimation and photoadaptation an response to environmental gradients in a sea shelf. Limnol. Oceanogr. **51**: 939–949. doi: 10.4319/lo.2006.51.2.0936

Oxborough, K., C. M. Moore, D. J. Suggett, T. Lawson, H. G. Chan, and R. J. Geider. 2012. Direct estimation of functional PSII reaction center concentration and PSII electron flux on a volume basisi: A new approach to the analysis of fast repletion rate fluorometry (FRRf) data. Limnol. Oceanogr. Methods **10**: 142–154. doi: 10.4319/lom2012.10.142

R Development Core Team. 2011. R: A language and environment for statistical computing. R Foundation for Statistical Computing, Vienna, Austria. Available at: http://www.R-project.org/.

Rijstenbil, J. W. 2003. Effects of UVB radiation and salt stress on growth, pigments, and antioxidative defence of the marine diatom *Cylindrotheca closterium*. Mar. Ecol. Prog. Ser. **254**: 37–47. doi: 10.3354/meps254037

Ritchie, R. J. 2006. Consistent set of spectrophotometric chlorophyll equations for acetone, methanol and ethanol solvents. Photosynth. Res. **89**: 27–41. doi: 10.1007/s11120-006-9065-9

Röttgers, R., and R. Doerffer. 2007. Measurements of optical absorption by chromophoric dissolved organic matter using a point-source integrating-cavity absorption meter. Limnol. Oceanogr. Methods **5**: 126–135. doi: 10.4319/lom.2007.5.126

Röttgers, R., and S. Gehnke. 2012. Measurement of light absorption by aquatic particles: Improvement of the quantitative filter technique by use of an integrating sphere approach. Appl. Opt. **51**: 1336–1351. doi: 10.1364/AO.51.001336

Röttgers, R., C. Hase, and R. Doerffer. 2007. Determination of the particulate absorption of microalgae using a point-source integrating-cavity absorption meter: Verification with a photometric technique, improvements for pigment bleaching, and correction for chlorophyll fluorescence. Limnol. Oceanogr. Methods **5**: 1–12. doi: 10.4319/lom.2007.5.1

Schreiber, U., C. Klughammer, and J. Kolbowski. 2012. Assessment of wavelength-depedent parameters of photosynthetic electron transport with a new type of multicolor PAM chlorophyll fluorometer. Photosynth. Res. **113**: 127–144. doi: 10.1007/s11120-012-9758-1

Shoaf, W. T., and B. W. Lium. 1976. Improved extraction of chlorophyll a and b from algae using dimethyl sulfoxide. Limnol. Oceanogr. **21**: 926–928. doi: 10.4319/lo.1976.21.6.0926

Silsbe, G. M., R. E. Hecky, and R. E. H. Smith. 2012. Improved estimation of carbon fixation rates from active fluorometry using spectral fluorescence in light-limited environments. Limnol. Oceanogr. Methods **10**: 736–751. doi: 10.4319/lom.2012.10.736

Silsbe, G. M., and J. C. Kromkamp. 2012. Modeling the irradiance dependency of the quantum efficiency of photosynthesis. Limnol. Oceanogr. Methods **10**: 645–652. doi: 10.4319/lom.2012.10.645

Strzepek, R. F., and P. J. Harrison. 2004. Photosynthetic architecture differs in coastal and oceanic diatoms. Nature **431**: 689–692. doi: 10.1038/nature02890

Suggett, D. J., E. Le Floc'H, G. N. Harris, N. Leonardos, and R. J. Geider. 2007. Different strategies of photoacclimation by two strains of *Emiliana huxleyi* (haptophyta). J. Phycol. **43**: 1209–1222. doi: 10.1111/j.1529-8817.2007.00406.x

Suggett, D. J., S. C. Maberly, and R. J. Geider. 2006. Gross photosynthesis and lake community metabolism during the spring phytoplankton bloom. Limnol. Oceanogr. **51**: 2064–2076. doi: 10.4319/lo.2006.51.5.2064

Suggett, D. J., H. L. MacInytre, and R. J. Geider. 2004. Evaluation of biophysical and optical determinations of light absorption by photosystem II in phytoplankton. Limnol. Oceanogr. Methods **2**: 316–332. doi: 10.4319/lom.2004.2.316.

Suggett, D. J., H. L. MacIntyre, T. M. Kana, and R. J. Geider. 2009. Comparing electron transport with gas exchange rates between alternative photosynthetic currencies for eukaryotic phytoplankton. Aquat. Microb. Ecol. **56**: 147–162. doi: 10.3354/ame01303

Suggett, D. J., C. M. Moore, and R. J. Geider. 2010. Estimating aquatic primary productivity using active fluorescence, p.103–128. *In* D. J. Suggett, O. Prasil, and M. A. Borowitzka [eds.], Chlorophyll *a* fluorescence in aquatic sciences: Methods and applications. Springer.

Tassan, S., and G. M. Ferrari. 1995. An alternative approach to absorption measurements of aquatic particles retained on filters. Limnol. Oceanogr. **40**: 1358–1368. doi: 10.4319/lo.1995.40.8.1358

Webb, W. L., M. Newton, and D. Starr. 1974. Carbon dioxide exchange of *Alnus rubra*: A mathematical model. Oecologia **17**: 281–291. doi: 10.1007/BF00345747

Wollschläger, J., M. Grunwald, R. Röttgers, and W. Petersen. 2013. Flow-through PSICAM: A new approach for determining water constituents absorption continuously. Ocean Dyn. **63**: 761–775. doi: 10.1007/s10236-013-0629-x

Received 12 August 2014
Revised 29 December 2014
Accepted 20 January 2015

Associate editor: Dr. Todd Kana